RICE UNIVERSITY

Impact of Surface Topography on Colloidal and Bacterial Adhesion

by

Jianwei Ma

A THESIS SUBMITTED

IN PARTIAL FULFULLMENT OF THE

REQUIREMENTS FOR THE DEGREE

Master of Science

Approved, Thesis Committee:

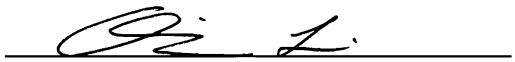

Qilin Li, Assistant Professor, Chair
Civil and Environmental Engineering, Rice University

Jun Lou, Assistant Professor
Mechanical Engineering and Materials Science, Rice University

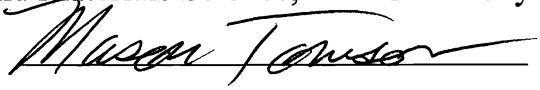

Mason B. Tomson, Professor
Civil and Environmental Engineering, Rice University

HOUSTON, TEXAS

NOVEMBER 2010

ABSTRACT

Impact of Surface Topography on Colloidal and Bacterial Adhesion

by

Jianwei Ma

Although the importance of substrate surface topography in colloidal and bacterial adhesion is widely recognized, how it affects the adhesion process has been a controversial topic. In this study, the impact of surface topography on adhesion of biological (i.e., bacteria) and non-biological colloids was investigated using natural and engineered surfaces with well-defined surface topographic patterns.

Adhesion experiments using carboxylate modified latex (CML) microspheres of 4μm in diameter and *Psudomonas Aeruginosa* on the taro leaf of *Colocasia esculenta,* a plant known for its self-cleaning property similar to that of the lotus leaf, in a 100 mM NaCl solution at pH 4 under submerged conditions showed that nanoscale surface structures on the papilla of the *Colocasia esculenta* leaf surface resisted adhesion by both CML and *P. Aeruginosa*. This resistance to adhesion was found to be independent of the wetting condition of the surface, suggesting that the surface superhydrophobicity was not the reason for the observed lack of adhesion. Interfacial force mapping by atomic force microscopy (AFM) revealed markedly lower adhesion forces over the surface area covered by these nano-structures where adhesion resistance was observed.

Adhesion experiments were also performed using 6 μm CML particles on

engineered micro-patterns fabricated on silicon wafers. The micro-patterned surfaces consisted cuboid pillars or pits of a wide range of sizes arranged at various spacings. Adhesion of CML particles on all micro-patterned surfaces was significantly less than on the smooth control surface. In general, adhesion decreased with decreasing pillar or pit size and spacing between the features. Adhesion was minimum on the micro-patterned surface when the dimension (pillar size) of patterns is close to/smaller than the size of the colloid when spacing between pillars was fixed to a size a bit smaller than the particle size; while the adhesion on patterns with fixed pillar size (a bit smaller than the particle size) was low for a wide range of spacings. Analysis of the spatial distribution of adhered particles on the pillar-patterned surfaces showed that more than 98% of the particles adhered on the edge of the pillars (between the pillars) when the spacing between pillars was smaller than the particle diameter; the particles adhered in the valley close to the pillars when the spacing was larger than the particle diameter. The characteristic adhesion distribution of the colloidal particles on the micro-patterned surfaces was also validated by the AFM adhesion force mapping: when spacing between pillars was smaller than the particle size, adhesion force was larger on the edge of the pillars; when spacing between pillars was larger than the particle size, adhesion force was larger on the valley. However, the AFM results could not explain the reduced adhesion on the patterned surface compared to the smooth surface.

ACKNOWLEDGEMENT

I would first like to thank my advisor and mentor, Dr. Qilin Li, for her invaluable guidance, patience, encouragement and great care, who has had a profound effect over my professional development. Without her, this work can never be possible. I wish to express my sincere gratitude to Dr. Mason Tomson for sharing his knowledge and advice and providing guidance, comments and critiques through the process. Additionally, I would like to sincerely thank Dr. Jun Lou and his group members for their collaboration and contributions to the pattern fabrication and AFM force measurement work presented in this thesis.

Thanks Bo Chen for the help in the XPS analysis.

I thank my research group for their continued feedback and encouragement.

I would like to thank my Mom, Dad, Sister and my friends for their continuous encouragement and love all the time.

Finally I would like to thank my wife, Zhe Mo, for her constant support, love, patience, words of comfort, who encourages me to face everything I meet.

This study was supported by the Center for Biological and Environmental Nanotechnology, as well as Shell Center for Sustainability at Rice University.

TABLE OF CONTENTS

LIST OF TABLES

LIST OF FIGURES

1. Introduction

1.1 Motivation and Background

Adhesion of biological (e.g., bacteria) and non-biological particles on surfaces in contact with water could cause serious problems in a wide range of applications, such as fouling of naval ship hulls[1] and membrane water filtration systems[2-4], underwater sensor contamination, clogging and corrosion of water distribution pipelines and reservoirs, contamination of food processing equipment, medical devices[5] and biomedical implants[6-8], everyone of which has significant economic and/or human health implications. For example, damages in industrial systems due to biofouling and biocorrosion amount to ~200 billion dollars annually in the USA alone[9].

Colloidal/bacterial adhesion is a complex process determined by many factors, such as the characteristics of the colloid or bacterium, the solution condition, and the physicochemical properties of the material surface including charge, hydrophobicity and surface topography[10].

Much research has been done on the surface chemistry effect on colloidal/bacterial adhesion[11-15]; more recently, attention has been turned to the effect of surface physical properties, such as topography or roughness[16-18].

Although a number of studies have investigated the impact of surface topography on colloidal/bacterial adhesion[16, 19, 20], conclusions from these studies are

contradictory and the mechanisms involved are unclear. For quite a while, surface roughness was believed to increase bacterial adhesion; however opposite observations have been reported in more recent studies[10, 20-26]. The usually poorly defined substrate surfaces and inadequately characterized topographies used are most likely responsible for such discrepancies. Meanwhile, well defined topographical structures have been demonstrated to resist bio-fouling[27-36], including fouling caused by zoospores of alga Ulva, mammalian cells and astroglial cells, but the reason for such resistance is unknown.

1.2 Objectives and Scope

The overall objective of this research is to systematically elucidate the effect of micro- and nano-scale surface topographic features on colloidal and bacterial adhesion. The specific aims include:

a.) To examine the role of surface topographic features in colloidal and bacterial adhesion on the surface of *Colocasia esculenta* (taro) leaf, a natural fouling-resistant surface due to its superhydrophobicity;

b.) To investigate how the physical properties of surface topographic features affect the adhesion of microscopic particles;

c.) To understand the mechanisms through which surface topographic features affect colloidal/bacterial adhesion.

1.3 Organization of thesis

This thesis is organized into six chapters. Following the Introduction, Chapter 2 presents a comprehensive literature review on fouling problems in environmental engineering systems, physicochemical interactions that control colloidal/bacterial adhesion, effects of surface topography on colloidal/bacterial-surface interactions and biological responses, methods for surface pattern fabrication, techniques for studying colloid/bacterial-surface adhesion, and theories currently used to describe the colloidal/bacterial adhesion process. Chapter 3 describes materials and methods used in this study, including test surface, model particles and bacteria, and experimental methods for quantification of colloidal/bacterial adhesion and measurement of adhesion forces. Chapter 4 and 5 present results from the studies on colloidal and bacterial adhesion on the surface of *Colocasia esculenta* leaf and micro-patterned silicon wafers, respectively. Chapter 6 compares calculated DLVO interaction energies on smooth and micro-patterned surfaces.

2. Literature Review

2.1 Fouling problems in environmental engineering systems

Fouling due to accumulation of biological and non-biological particles is a serious problem in many environmental engineering applications. For example, particulate or bio-fouling of water filtration membranes leads to decline in membrane permeate flux and hence higher energy consumption for pumping. The lower membrane permeate flux requires more frequent chemical cleaning, which significantly reduces production rate and increases maintenance cost. Over time, the fouling-chemical cleaning cycles also cause deterioration of the membrane material, resulting shorter membrane lifetime. Biofouling in water distribution systems can cause clogging and corrosion of water distribution pipelines, resulting in higher pumping energy, leakage or breakage of the water pipes; the formation of biofilms in water distribution systems can also harbor pathogens and cause secondary contamination through processes such as nitrification. Underwater monitoring sensors usually have limited lifetime because of interference caused by particle and bacterial fouling. Therefore, it is of great significance to understand adhesion of biological and non-biological particles on material surfaces in order to design rational countermeasures against fouling.

2.2 Physicochemical Interactions controlling colloidal/bacterial adhesion

Particle (both biological and non-biological) deposition on solid surfaces can be regarded as a two-step process: (i) the particles are transported close to the adhesive surface, and (ii) adhesion takes place under the control of physicochemical interactions and shear forces[37].

Two sequential steps are involved in the bacterial adhesion process: the initial attachment phase, a quick, reversible step controlled by the physicochemical interactions between the bacterial cell and the substrate surface, and the irreversible adhesion step involving specific biochemical interactions between the bacterial surface macromolecules and the substrate surface.

The same physicochemical interactions are involved in the initial attachment step for both colloidal and bacterial adhesion. They include both long-range interaction forces, such as electric double layer interactions and van der Waals forces, and short-range interactions, such as dipole interactions, chemical (i.e., covalent and hydrogen) bonding, and hydrophobic interactions[38, 39].

2.2.1 Factors affecting colloidal/bacterial adhesion

Many factors determine the physicochemical interactions involved in the initial attachment step, such as the characteristics of the colloidal particle or bacterium, the solution chemistry, and the surface properties of the substrate including surface chemical composition, charge, solidity, curvature, hydrophobicity and surface

topography[10].

Bacterial adhesion can be affected by the substrate surface property via influencing the protein adsorption and/or altering the conformation of the adsorbed protein. When bacterial adhesion is not mediated by extracellular proteins, it can be affected by surface properties via van der Waal forces, electrostatic interactions between the negatively charged bacterial surface and the surface, and other forces[40] such as acid-base forces (including hydrophobic forces). While much attention has been paid to the effects of surface chemistry, hydrophobicity, charge and surface energy on bacterial adhesion, relatively little work has been done to elucidate the role of surface topography.

Extracellular polymeric substances (EPS) play an important role in bacterial adhesion. Satoshi Tsuneda et al.[41] found that polymeric interactions due to the EPS associated with the cell surface promoted bacterial cell adhesion.

Solution chemistries, such as total ionic strength[42-44], pH values[45] and the presence of cationic species, including iron[46, 47], cadmium and zinc[48] etc also influence bacterial adhesion.

2.2.2 Existing theoretical models for colloidal/bacterial adhesion

Colloids are defined as particles microscopically dispersed evenly throughout a certain solvent medium. A colloidal system consists of two separate phases: a dispersed phase (or internal phase) and a continuous phase (or dispersion medium). A colloidal system may be solid, liquid, or gaseous. The generally accepted size range of

colloids is fairly wide, from particles a couple nanometers in diameter to particles about 50 μm in diameter. Since the size of most bacteria is in the range of 500nm to 10 microns, bacteria can also be considered biological colloids. Therefore, theories for colloidal systems have been applied to bacteria with varying degrees of success.

Two theoretical approaches have applied to describe the initial colloidal/bacterial attachment. Both methods were originally developed for smooth surfaces.

2.2.2.1 The DLVO Approach

The DLVO theory, developed by Derjaguin and Landau[49], Verwey and Overbeek[50-52], is the most commonly used theory for colloidal stability. The classical DLVO theory is based on the ideal condition of smooth particle or flat surface (geometrically smooth and chemically homogeneous), and it only considers the van der Waals forces and electrostatic forces. The classical DLVO theory simply states that the total interaction energy between two surfaces is the summation of van der Waals attractive energy and electrostatic interaction energy. It is based on the ideal condition of geometrically smooth particles or planar surfaces. Much effort has been made to modify the classical DLVO theory to account for other interactions[53-57] (e.g. acid-base interactions); modifications have also been made to describe the interactions between rough surfaces[56, 58-61].

van der Waals Forces. The van der Waals forces include dipole-dipole force, dipole-induced dipole force and dispersion forces[62], among which dispersion forces are the most important because they are always present. The van der Waals force interaction energy between a sphere and a plate can be calculated by the following

equation

$$U(D) = -\frac{AR}{6D} \qquad (2.1)$$

Where A is the Hamaker constant (J), which is experimentally obtained for various systems; R is the radius of the sphere; D is the distance between the sphere and the plate.

(2). Electrostatic Forces

Electrostatic forces between two charged surfaces in solution arise from the formation of an electrical double layer (EDL), as shown in Figure 2.1. When a surface is placed in an aqueous solution, the surface usually becomes charged due to ionization, metal ion substitution or ion adsorption. Because of this net charge, the surface draws in ions with charges of the opposite sign, which would otherwise be randomly distributed in the solution. Meanwhile, the surface repels same sign charges in the solution. This leads to an electric potential (ψ) that declines from the value at the surface (ψ_0) to zero in the bulk solution.

To calculate ψ as a function of distance from a charged planar surface (x), two basic equations are used, the Boltzmann equation of statistical mechanics (Eq.2.2) and the Poisson equation (Eq.2.3), derived directly from the Maxwell equations of electrodynamics.

$$n_i = n_{i\infty} \exp(-\frac{E}{kT}) \approx n_{i\infty} \exp(-\frac{Z_i e\psi}{kT}) \qquad (2.2)$$

$$\nabla^2\psi = -\frac{\rho_e}{\varepsilon} \qquad (2.3)$$

Here, n_i (particles/volume) is the number concentration of ion i, $n_{i\infty}$ (particles/volume)[63] is the number concentration of ion i in the bulk solution, E is

the energy of an ion (J), k is the Boltzmann constant (1.38×10^{-23} J/K), T is the absolute temperature in Kelvin, Z_i is the valence of ion i, e is the charge of a proton (1.6×10^{-19} C), ρ_e is the charge density (C/m^3), and ε is the permittivity of the solution (C^2/Nm^2). When these two equations are combined, non-dimensionalized by $\phi = Ze\psi / kT$, the Poisson-Boltzmann equation is obtained:

$$\frac{d^2\phi}{dx^2} = \kappa^2 \sinh\phi \qquad (2.4)$$

where $\kappa^2 (= \frac{2n_\infty Z^2 e^2}{\varepsilon kT})$ (2.5)

When assuming that $\sinh\phi = \phi$ (a good approximation when ϕ value is small), the solution to Equation 2.4 is called the Debye-Huckel approximation

$$\psi = \psi_0 e^{-\kappa x} \qquad (2.6)$$

The Debye length, $1/\kappa$, is the characteristic decay length of the electrostatic potential into the solution. As can be seen from the Eq.2.5, the Debye length decreases by a factor of 10 with a 100-fold increase in ion concentration (n_∞). Electrostatic forces play a more significant role in solutions when ionic strength is small (generally less than 1 mM), but are not as significant in solutions of high ionic strength (more than 50 mM)[63].

For a spherical particle, this equation becomes Eq.2.7, in which l is the distance from the center of the sphere, and r is the radius of the sphere.

$$\psi = \psi_0 \frac{\exp(-\kappa(l-r))}{l/r} \qquad (2.7)$$

For identical spheres (same radius and surface potential), the electrostatic potential between them can be calculated by Eq. 2.8, where r is the radius of each

sphere, and δ is the distance separating them. The force between two spheres can be calculated by Eq. 2.9.

$$\Phi_{ss} \approx 2\pi\varepsilon\psi_0^2 r\, e^{-\kappa\delta} \qquad (2.8)$$

$$F_{ss} = 2\varepsilon\kappa^2\psi_0^2 e^{-\kappa\delta} \qquad (2.9)$$

As can be seen in Eq. 2.9, the force decays exponentially with distance. Because the value of $1/\kappa$ is typically in the range of 1 to 100 nm, the effects of electrostatic interactions can usually be neglected beyond 100 nm from a charged surface[63].

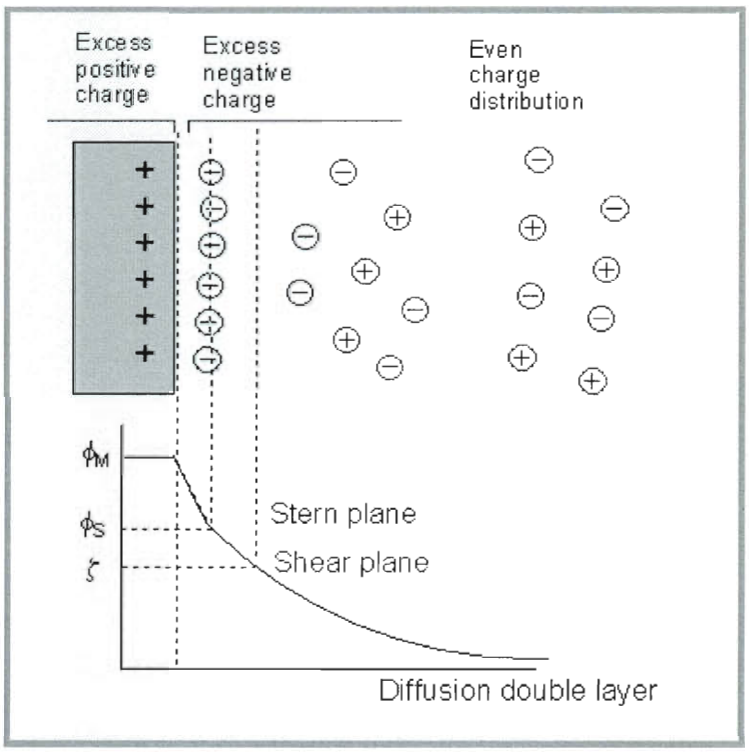

Figure 2. 1. The Electrical Double Layer (EDL).

Extended DLVO theory. While the DLVO theory provides a robust explanation for the stability of lyophobic colloids, there are many reported discrepancies between

experimental observations of particle stability, deposition and adhesion in natural and engineered systems and DLVO predictions. To reconcile such discrepancies, some researchers have considered non-DLVO interactions, such as acid-base (including hydrophobic forces)[64], depletion, steric[65] and hydrodynamic forces[66, 67]. Addition of any non-DLVO interactions to van der Waals and electrostatic forces can be considered as an "extended DLVO" or "XDLVO" approach.

When considering Lewis acid-base (AB) interactions[68, 69]. The total XDLVO interaction energy per unit area between two infinite planar surfaces can be expressed as follow:

$$E_{PP}^{XDLVO}(h) = E_{PP}^{LW}(h) + E_{PP}^{EL}(h) + E_{PP}^{AB}(h) \tag{2.10}$$

The interaction energies for each individual component-LW, EL and AB-are given by:

$$E_{pp}^{LW}(h) = -\frac{A_H}{12\pi h^2} \tag{2.11}$$

$$E_{pp}^{EL}(h) = \varepsilon\varepsilon_0\kappa\psi_p\psi_m[\frac{\psi_p^2+\psi_m^2}{2\psi_p\psi_m}(1-\coth(\kappa h)) + \frac{1}{\sinh(\kappa h)}] \tag{2.12}$$

$$E_{pp}^{AB}(h) = \Delta G_{h_0}^{AB}\exp(\frac{h_0-h}{\lambda}) \tag{2.13}$$

$$A_H = -12\pi h_0^2 \Delta G_{h_0}^{LW} \tag{2.14}$$

$$\Delta G_{h_0}^{LW} = 2(\sqrt{\gamma_w^{LW}} - \sqrt{\gamma_m^{LW}})(\sqrt{\gamma_p^{LW}} - \sqrt{\gamma_w^{LW}}) \quad (2.15)$$

$$\Delta G_{h_0}^{AB} = 2\sqrt{\gamma_w^+}(\sqrt{\gamma_m^-} + \sqrt{\gamma_p^-} - \sqrt{\gamma_w^-}) + 2\sqrt{\gamma_w^-}(\sqrt{\gamma_m^+} + \sqrt{\gamma_p^+} - \sqrt{\gamma_w^+}) - 2(\sqrt{\gamma_m^+\gamma_p^-} - \sqrt{\gamma_m^-\gamma_p^+}) \quad (2.16)$$

Among which, A_H is the particle-substrate Hamaker constant in water, $\Delta G_{h_0}^{LW}$ is the Lifshitz-van der Waals free energy per unit area at contact between a planar surface (m) and a particle (p) surfaces interacting in water (w), $\gamma_w, \gamma_m, \gamma_p$ are interfacial energies of water, the planar surface and particle respectively; $h_0 = 0.158$ nm is the minimum separation distance due to Born repulsion[70], $\Delta G_{h_0}^{AB}$ is the acid-base free energy per unit area between the particles and surfaces at contact, $\lambda = 0.6\,nm$ is the decay length for acid-base interactions in water, $\varepsilon = 78.5$ is the dielectric constant of water, κ is the inverse Debye length, and ψ_p and ψ_m are the surface potentials for the particle and planar surface.

In some cases, polar (hydrophobic), steric, capillary, and hydration interaction forces were also considered to explain experimental phenomena.

DLVO/XDLVO with topographic consideration. In addition to non-DLVO interactions, physical heterogeneity, i.e., roughness, has been implicated as the cause of discrepancies between DLVO (or XDLVO) predictions and experimental results[57, 71, 72].Theoretical work that considered the effect of surface topography is summarized in section 2.3.

2.3 Effect of surface topography on colloidal/bacterial-surface interaction

2.3.1 Overview

Extensive experimental studies in biomaterial science and clinical applications such as orthopedic, dental and cardiovascular prosthesis[73-75] have demonstrated the role of surface topography on cell adhesion behavior, although randomly rough/ porous surfaces were often used.

2.3.2 Physicochemical interactions between colloids/bacteria and topographical surfaces

The first quantitative study considering the effect of a hemispherical asperity on the adhesion force of a smooth colloid particle was done by Krupp[76] and it concluded that the electrostatic component determines the net adhesion force due to its smaller decrease than the dispersion forces as distance increases. Adamczyk[77] used a similar model to determine the maximum size of a rough parcel adhering to an smooth interface under hydrodynamic shearing forces. An analogous model was used by Elimelech and O'Melia[78] to simulate the interaction between a smooth particle and a plate with a hemispherical asperity. The Derjaguin method was used to calculate the electrostatic interaction energy by summing the contributions of the particle/smooth surface and particle/asperity interactions. An additive principle was adopted by Czarnecki[79, 80] to model the interaction of a smooth sphere with a rough plate surface generated by distributing many small spherical particles with

different sizes. Large differences between interaction energies of the sphere and the interface were predicted at different separation distance, and used to explain the specific tangential interactions in particle adhesion. Herman[81, 82] adopted this additive principle to study the effect of conical and hemispherical asperities on the van der Waals and electrostatic interactions between planar surfaces using the linear superposition approach (LSA) and the Derjaguin method, and showed that repulsive interaction energy on the rough surface was increased compared to a smooth surface for the studied conditions adopted. This method has been generalized to the rough colloidal particle/smooth surface systems[60, 83].

To develop improved modes, Kostoglou et al[84] calculated electrostactic interactions of two infinite planar surfaces with periodic (sinusoidal) surface roughness, showing that the repulsive interaction energy for rough surfaces is larger than that for smooth surfaces; however a decrease in the electrostatic repulsive interaction energy upon contact was predicted based on the theory. On the contrary Suresh[60] showed that surface roughness extends the range and depth of the secondary minimum while decreasing the energy barrier.

Bowen et al[85] showed a greater repulsive interactions energy on the flat section than the peaks on a membrane surface. A study by Hoek et al[56] showed that on average extended DLVO potential is reduced by surface roughness due to the fact that particle-substrate separation is effectively larger, leading to a higher adhesion because van der Waals interactions are stronger at long range than either acid-base or electrostatic interactions. Another research done by the same group[61] on membrane

demonstrated that the repulsive energy barrier between a colloidal particle and a rough membrane was lower than that for a smooth membrane and that membrane surface roughness provided low energy positions in the valleys where more colloids would adhere.

Physicochemical interactions between the bacterial cells and the substrate surface controls the initial reversible attachment phase for bacterial adhesion. This is affected by the surface topography to a large extent[10], and was believed to depend more on the roughness than on the hydrophobicity or the charge of the solid surface[86, 87].

2.3.3 Biological response of bacterial cells to surface topography

2.3.3.1 Influence of micro-scale surface topography on cellular response

The effect of micro-scale surface on cellular response has long been recognized[88-90]. Micro- topographic structures have been shown to promote or inhibit bacterial adhesion, as well as to induce physiological changes of bacteria.

Komaromy et al[91] manufactured micro-structured pyramids of different sizes (base of 2, 3.5 or 5 μm^2) and spacings (4-64 μm; 6-96 μm; 10-160 μm) with different surface chemistry (unmodified, gold coated, hydrophilic modified and hydrophobic modified); they found that cell viability and adhesion were influenced by a combined effect of the zeta-potential and surface topography. Oh et al[92] created surfaces resistant to bacterial adhesion surface by micro-patterning BSA on glass and found that the size of the surface pattern was crucial for the anti-adhesion property. Research done by Diaz et al[93] showed that sub-microstructured surfaces on copper

and gold substrata influenced bacterial length, alignment and distribution as well as the shape of the bacterial colonies and the polymeric substances production.

Sometimes for a specific experimental system with micro-scale surface feature(s), it is difficult to decouple the role of various factors involved in bacterial adhesion such as surface chemistry, topography, adsorption of biomolecules, and cell-type-specific response[94].

2.3.3.2 Influence of nano-scale surface topography on bacterial cellular response

The nano-scale topography of man-made materials is known to play a role in interactions between cells (e.g. bacterial cells) and surfaces. A detailed understanding and ultimate manipulation of these interactions is of extreme importance in many different areas. Although bacterial cellular responses to nano-scale surface features have been widely reported[16, 32-34, 94], the underlying mechanisms of cell sensing, intercellular signaling and long-term response to surface nanotopography are still unclear and need to be addressed.

The influence of nanotopography on cellular response has been explored using a variety of surface topographies and cell types[95, 96]. Research done by Whitehead et al.[97] showed that nano-scale pitted structure could either decrease or increase bacterial adhesion compared with a smooth surface depending on the bacterial types. Inhibited cellular alignment, cell-cell adhesion and aggregation of *P. fluorescens* on ordered micro/nano structured patterns relative to a random nano-featured surface was reported by Diaz et al.[98].

So far the experimental observations of bacterial adhesion on

micro-/nano-structured surfaces are contradictory and sometimes misleading. A likely source of the contradiction is the random surface roughness structure as well as the difference in surface chemistry of the samples used for comparison. Well-defined surface topography with the same surface chemistry is needed to isolate and elucidate the role of surface topography in particle/bacterial adhesion.

2.3.4 Nature's solution to fouling

Nature is a very smart system, in which materials and structures with unique functions have been developed as a result of millions of years' evolutionary. Human beings can learn from the nature and apply biological methods and systems found in nature to the study and design of engineering systems and modern technology, which forms a new scientific area, bionics (or biomimetics)[99]. One of the terrific property human beings are imitating with extreme ardor because of its tremendous potential application in a wide range of different areas is the antifouling effect displayed by many plants, such as lotus leaf and taro and animals, such as shark and some birds.

2.3.4.1 Lotus effect

Lotus effect refers to the very high water repellency (superhydrophobicity) exhibited by the leaves of lotus leaf (*Nelumbo nucifera*) and other plants, such as taro leaf[100, 101]. Dirt particles on the lotus leaf surface can be picked up easily by water droplets due to a complex hierachical structure of the surface, i.e. micrometer-sized bumps and nanoscale hair-like structures, which minimizes contact and enhances hydrophobicity and hence which resists particle adhesion (Figure 2.2).

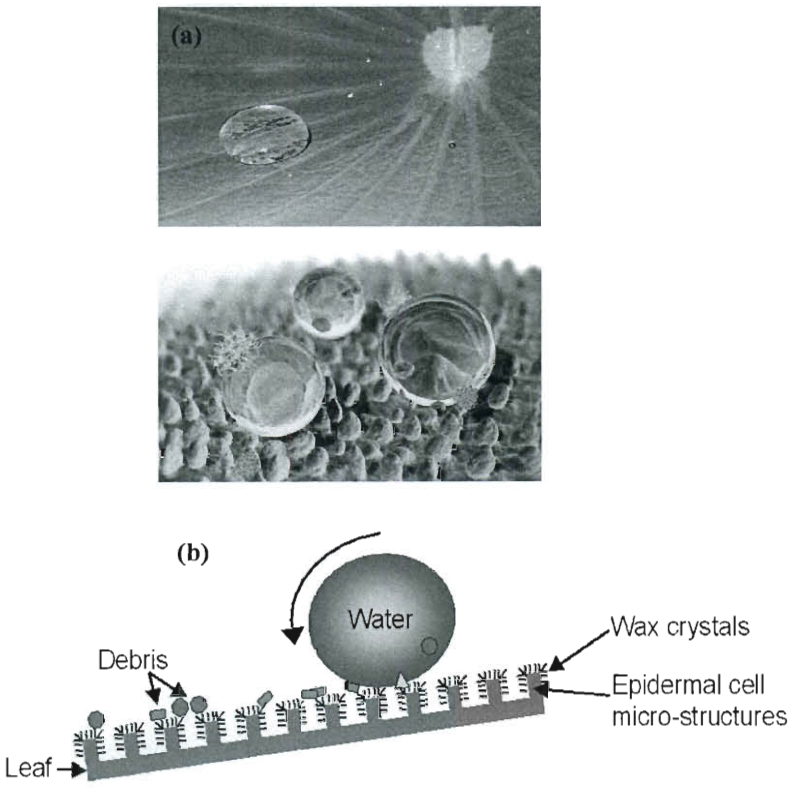

Figure 2. 2. Water drop on lotus leaf (a); schematics of lotus effect (b).
(http://www.thenakedscientists.com/HTML/articles/article/biomimeticsborrowingfrombiology/)

2.3.4.2 Shark skin

The skin of sharks exhibits a rather intriguing three-dimensional rib pattern[102] (Figure 2.3). The very small individual tooth-line scales of shark skin, called dermal denticles (little skin teeth), are ribbed with longitudinal grooves (aligned parallel to the local flow direction of the water), which results in water moving very efficiently over their surface. Because of this unique structure, the drag force can be dramatically reduced when sharks swim in the sea. Further more, this textured film provides a self-cleaning function: the rough surface confers low contaminant/organism adhesion

(fouling). Unlike the superhydrophobic lotus leaf surface, the shark skin is hydrophilic and wets with water[99]. There are three factors that appear to help keep the shark skin clean: (1) reduced contact time of fouling stuff due to the accelerated water flow at the shark's surface , (2) reduced surface area for adhering organisms and unstable surface repellant to microbes due to the nano-structure, and (3) "unstationary target" created by the realigned and flexed scales of shark[103].

Replication of shark skin has been used to develop moving objects with low drag, e.g. whole body swimsuits (Speedo swimsuit). Novel engineered surfaces for medical devices, healthcare and marine environments modeled after shark skin have also been developed with certain success recently[27, 29-31, 104, 105] (Figure 2.4), which can reduce the incidence of microorganism adhesion. New surface coatings for boats with this emulated shark skin texture have been shown to reduce fouling by marine organisms, such as barnacles by 67% over conventional surfaces[106].

Skin of other sea animals, such as whales also shows the ability of self-cleaning through similar mechanisms as those for the shark skin[107].

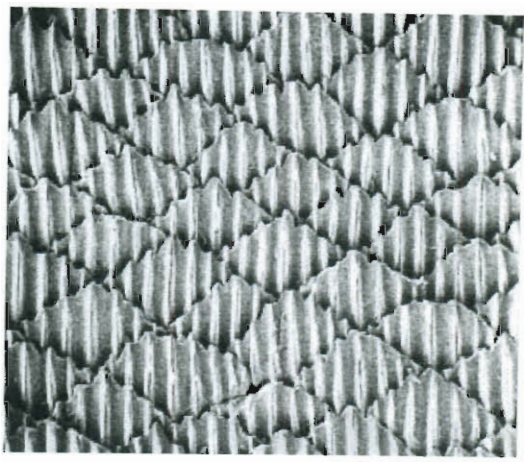

Figure 2. 3. Riblet pattern on shark skin[108].

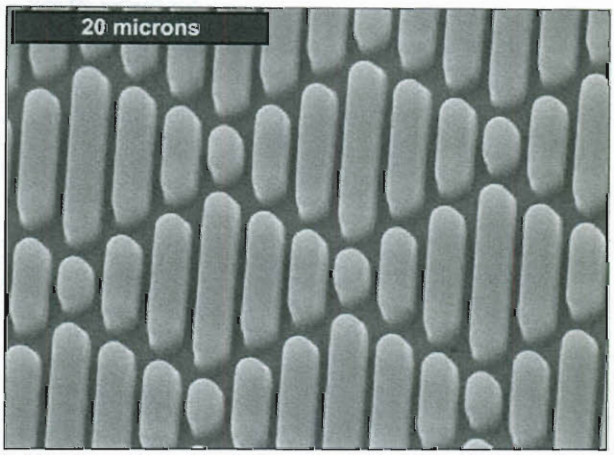

Figure 2. 4. Synthetic sharkskin pattern-Sharklet^{TM}

2.3.4.3 Animal wing

Wings of some birds and insects[109] appear to prevent adhesion and stay clean[110]. Feathers on many birds' wings exhibit hydrophobicity and low adhesion of debris. Figure 2.5 shows the SEM image of the pigeon feather (pennae)[111].

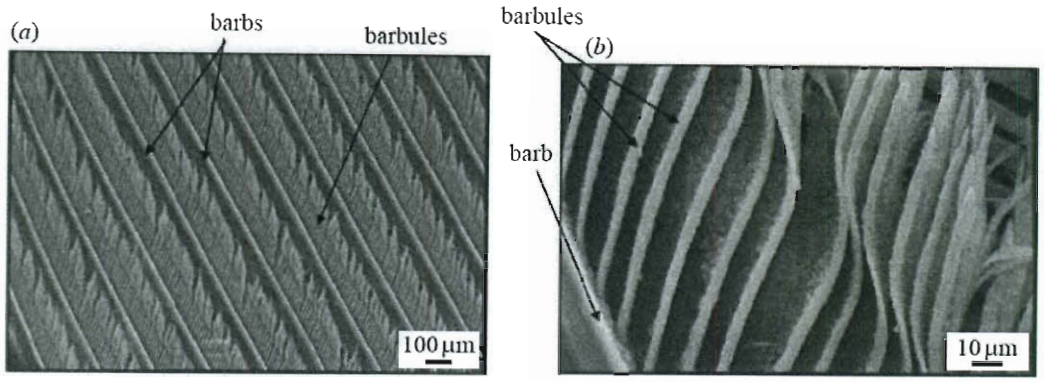

Figure 2. 5. SEM images of pigeon feather structure at two different magnifications

It is the morphology that plays an important role in water repellency and low adhesion. For example, the specific nanostructure enhances the hydrophobicity of butterfly wings (Figure 2.6), which allows droplets of water to scroll easily over the wing surface, removing the dust particles easily[112].

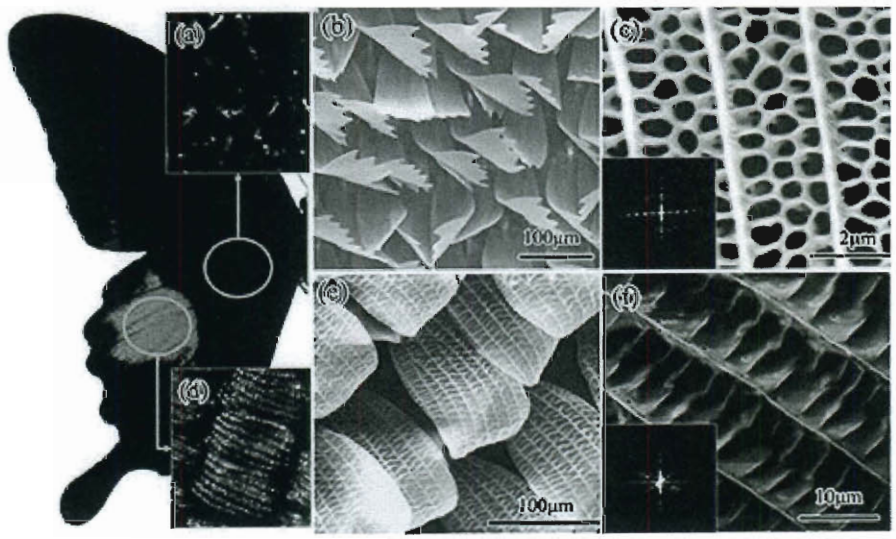

Figure 2. 6. Butterfly wing and its surface structure

2.3.4.4 Petal effect

Hierarchical micropapillae and nanofolds that exist on the petal surface of a

flower such as red roses (Figure 2.7), result in superhydrophobicity and thus self-cleaning properties[113].

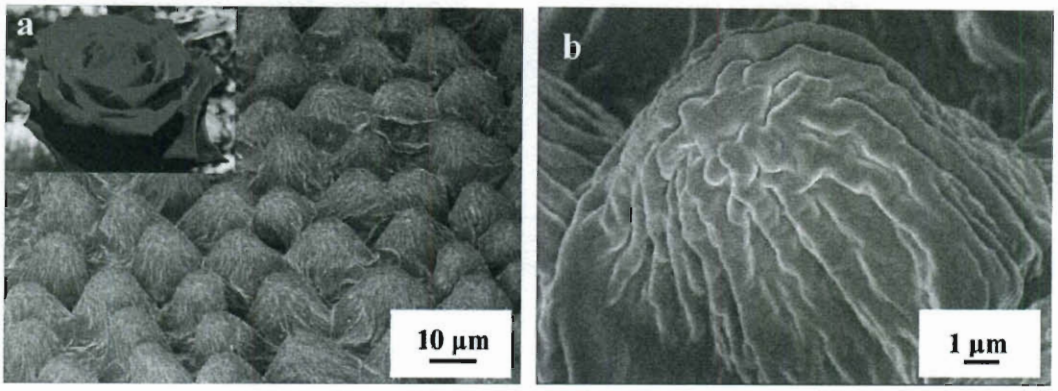

Figure 2. 7. Micropapillae and nanofolds structure on the surface of a red rose petal[113]

2.3.4.5 Insect legs

Legs of some insects, such as water striders[114] are covered by unique hierarchical surface structures, consisting of large numbers of oriented tiny hairs (microsetae) and fine nanogrooves (Figure 2.8). These surface structures render water resistance, which helps lower particle contamination.

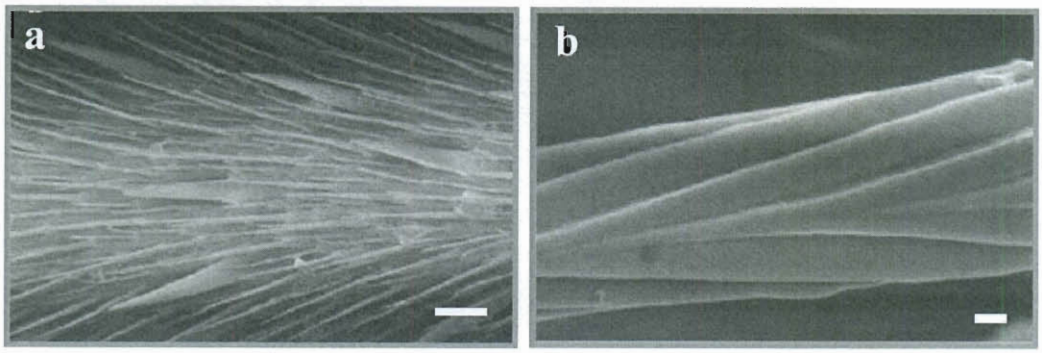

Figure 2. 8. SEM image of a water strider leg showing spindly microsetae (a) and fine nanoscale grooved structures on a seta (b). Scale bar: a, 20μm; b, 200nm.

2.4 Engineered surface topography

In-depth studies on the relationship between surface topography and colloidal/bacterial adhesion were made possible by means of micro- and nano-fabrication, adapted from the electronics industry, which provides a very wide range of very precisely defined topographies. A couple of review papers have summarized the fabrication methods and effects of micro- and nano-patterned surfaces on colloidal/bacterial adhesion[115, 116].

Increased efforts have been made in the past ten years to develop new fabrication technologies which allow production of structured surfaces with greater geometrical complexity at reduced operation time and cost[115]. To fabricate well controlled ordered patterned surfaces, it is essential to focus on the following aspects: (i) highly reproducible micro-/nano-features, (ii) surfaces with uniform and coherent micro-/nano-structures over large area, (iii) fast fabrication, (iv) uniform chemistry.

2.4.1 Micro-scale patterned surface fabrication approach

Micro-structured surfaces have been successfully made widely by many researchers all over the world via various methods, including photolithography, X-Ray lithography, laser scanning, wet bulk micromachining, serial writing with charged particles, focused ion beam, direct writing and material deposition, self-assembly of block copolymers etc[117].

2.4.1.1 Photolithography

Also called optical lithography used in microfabrication to selectively remove parts of a thin film or the bulk of a substrate, is a process of transferring geometric pattern from a photo mask to a light-sensitive chemical photo resist, or simply 'resist' on the substrate by selectively removing parts of the resist or the bulk of a substrate. A series of chemical treatments engraves the exposure pattern into the material underneath the photo resist. The steps involved in the photolithographic process are wafer cleaning; barrier layer formation; photoresist application; soft baking; mask alignment; exposure and development; and hard-baking.

In many photolithographic process cases, reactive ion etching (RIE) is used. RIE uses chemically reactive plasma to remove material deposited on wafers. The plasma is generated under low pressure (vacuum) by an electromagnetic field; high-energy ions from the plasma attack the wafer surface and react with it.

2.4.1.2 X-Ray Lithography

X-ray lithography uses X-rays to transfer a geometric pattern from a mask to a light-sensitive chemical photoresist on the substrate. X-Ray lithography is superior to

optical lithography because of the use of shorter wavelengths (below 1 nm) overcoming the diffraction limits of optical lithography, allowing smaller feature sizes; meanwhile, it has very large depth of focus and also exposure time and development conditions are not as stringent as photolithography. Reproducibility is high as results are independent of the substrate type, surface reflections, and wafer topography. With an X-ray wavelength on the order of 10 Å or less, diffraction effects generally are negligible and proximity masking can be used, increasing the lifetime of the mask. With a standard 50 μm proximity gap and using synchrotron X-rays one can print 0.25 μm patterns; by decreasing the proximity gap to 25 μm, patterns of 0.15 μm can be achieved[118, 119]. Deep X-ray lithography (DXRL) uses yet shorter wavelengths on the order of 0.1 nm and modified procedures such as the LIGA process, to fabricate deep and even three-dimensional structures. The obtainable aspect ratio, defined as the structural height or depth over the minimum lateral dimension, reaches more than 100. In contrast, an aspect ratio of about ten is possible under special condition with UV photolithography.

2.4.1.3 Laser Scanning

Laser scanning, a maskless technique, uses UV, nanosecond pulsed excimer, and Nd: YAG lasers to scan the resist surface. Pico-second and femto-second lasers have raised interest recently by enabling 3D structuring with higher precision in a single step using two-photon polymerizable systems. These techniques can be applied to pattern larger areas than possible with photolithography. Since they also rely on photoactivation and development of resist layers, the same issues concerning coating,

development, and rinsing also apply to laser scanning. Stereolithography by scanning resist multilayers[120] and two-photon lithography[121] have been developed based on the fundamental laser scanning.

2.4.1.4 Wet bulk micromachining

In wet bulk micromachining, features are sculpted in the bulk of materials such as silicon, quartz, SiC, GaAs, Inp, Ge, and glass by orientation-dependent (anisotropic) and /or by orientation-independent (isotropic) wet etchants. Wet etching typically uses alkaline liquid solvents, such as potassium hydroxide (KOH) or tetramethylammonium hydroxide (TMAH) to dissolve silicon which has been left exposed by the photolithography masking step. The technology employs pools as tools[122] instead of the plasmas. A vast majority of wet bulk micromachining work is based on single crystal silicon, some on crystalline Ge and GaAs, and a minor amount on GaP, InP, an SiC. Micromachining has grown into a large discipline, comprising several tool sets for fashioning microstructures from a variety of materials. These tools are used to fabricate micro-structures either in parallel or serial processes.

2.5 Techniques for Studying Colloid/Cell-surface Adhesion

A complete understanding of mechanisms of colloidal/cell adhesion is yet to come forth. Various experimental techniques have been developed to study colloidal/cell adhesion[123]. Most of the techniques adopted impose external forces to colloids/cells existing on investigated surfaces and then measure the force, energy or probability of attachment/detachment of many colloids/cells or single colloid/bacterial

cell or directly collected images of colloids/cells on surface. It is worth noting that a certain technique may only work for some specific colloid/cell types, substrate materials, surface conditions or particular experiment systems.

2.5.1 Batch Adhesion Experiment (BAE)

Batch adhesion experiment is a traditional method adopted by many researchers to study the colloidal/bacterial adhesion on different surfaces, which is a simple, inexpensive and straightforward system. The principle of this method is described as follows[124]: a prepared surface is soaked within a suspension of colloids/cells for a determined period of time (horizontal[125] or vertical[126] configuration; with[125] or without[126] mixing); afterwards, the non-adherent colloids/cells are removed by rinsing or centrifugation and the remaining (adhered) cells on the surface are counted. During rinsing, extremely large removal forces can be imposed onto the adhering colloids/bacteria[127]. For instance, it has been calculated that the removal forces involved in passing an adhering bacterium through a liquid-air interface are approximately 10^{-7} N[128, 129], whereas removal forces of around 10^{-9} to 10^{-10} N have been estimated for 'slight' rinsing with an aqueous fluid flow[130]. The exact value of these unintentionally exerted removal forces depends on individual operation and detailed experimental conditions; still it can be stated that the magnitude of these removal forces is in the same order as the interaction forces between bacteria and a surface[131].

The remaining (adhered) colloids/bacteria can be examined by a number of

methods, including[123]:

I. Microscopy for counting and morphological observation of adherent bacteria

- Light Microscopy
- Image-analysed epifluorescence microscopy (Imunofluorescence, Fluorescence *In Situ* Hybridisation[132, 133])
- Scanning Electron Microscopy (SEM)
- Scanning Confocal Laser Microscopy

II. Viable Bacterial Counting Methods

- CFU plate counting

This most basic method counts the number of bacteria in suspension (the difference between original bacterial number and after-adhesion bacterial number is the adhered bacterium number). Two basic ways were summarized by Herbert[134], the pour plate and surface spread method. This method has certain disadvantage such time consuming work as well as many variables due to indirect and complicated procedure.

- Radiolabelling

Three steps are included in this method, prelabelling bacterial cells with radiotracer such as [^{14}C] leucine[135, 136], [^{14}C] glucose[137], [^{3}H] thymidine[44], or [^{3}H] palmitic acid[138], bacterial adhesion process, and then scintillation counting. The advantages of this method include its usefulness for bacterial adhesion to irregular material surfaces[139, 140] and its sensitiveness, accurateness and rapidness. But there is potential risk to performers by the radioactive materials.

- CTC staining

The fluorescent redox dye 5-cyano-2,3-ditolyl tetrazolium chloride (CTC) has been used for direct visualization of respiring bacteria[141, 142]. CTC is colorless and does not fluoresce when oxidized, while forms fluorescent CTC-formazan when reduced by electron. CTC staining provides excellent visualization and quantification of actively respiring bacteria with the aid of image analyzing tool[143].

□. Other Direct and Indirect Methods

- Spectrophotometry

This method is based on the quantitative relation between optical density (from different staining techniques, such as crystal violet and Congo red) and colony counts derived from the standard curve. Two basic measuring techniques have been adopted (1) bacteria are washed off the substrata, stained in solution and the solution is examined in a spectrophotometer; (2) the bacterial adhered substratum is examined directly in a spectrophotometer after staining[144-146].

- Coulter Counter

This method first used by Kubitschek in 1958[147] for counting and measuring the size of bacteria measures the resistance of a conducting solution as a particle passes through an aperture. It was used to count the total number of bacteria while the colony counting was used to determine the viable bacterial counts[148].

- Biochemical Markers

One biochemical marker used to determine the viable cell counts is adenosine triphosphate (ATP) extracted from cell[149]. Bioluminescence ATP analysis has also

been reported by Harber et al. to assess bacterial adhesion with hydrophobic polystyrene tubes as the attachment surface[45].

DNA content measured with a fluorometric technique with Hoechst staining has also been used to evaluate the numbers of bacteria adhered to surfaces[150].

Lipopolysaccharide (LPS) content has also been reported as a marker for adhered bacteria[151].

The main disadvantage of the batch adhesion assay is it is a qualitative or semi-quantitative method because of the varying degree of detachment due to the uncontrollable imprecise rinsing[127]. Meanwhile, it is hard to control the hydrodynamics in the batch adhesion assay.

2.5.2 Atomic Force Microscope (AFM)

Two forces are included in the physicochemical interactions, i.e. normal force (or perpendicular force) and lateral force. Normal interaction forces have been well covered as to the bacterial adhesion study; however lateral force on which surface topography may have a more significant impact is rarely paid much attention and sometimes even ignored[152, 153].

2.5.2.1 Normal force

The atomic force microscope (AFM) system has evolved into a useful and standard tool for direct measurements of micro-structural parameters and unraveling the intermolecular forces at nano-scale level with atomic-resolution characterization. Another growing field is the use of the AFM as a nanomechanical sensor that allows

probing colloidal/cellular adhesion on different surfaces. The schematic of AFM is shown in Figure 2.9.

The AFM consists of a cantilever with a sharp tip (probe) at its end that is used to scan the specimen surface. The cantilever is typically silicon or silicon nitride with a tip radius of curvature on the order of nanometers. When the tip is brought into proximity of a sample surface, forces between the tip and the sample lead to a deflection of the cantilever according to Hooke's law,

$$F = k\delta \qquad (2.17)$$

F, force between the tip and sample; k, spring constant; δ, cantilever deflection.

A major advantage of the AFM over other microscopical techniques is that it can provide not only the information on local surface properties and also the interaction forces. Force measurements are made by recording the deflection of the cantilever while the sample is moved up and down. After proper corrections, a force-distance curve (Figure 2.10) is obtained in which the force experienced by the probe is plotted as a function of the probe-sample separation distance. Retract adhesion force will be used for the adhesion force measurement[154].

Although this technique gains powerful ability in detection, there are also concerns regarding the possible destructive deformation of bacterial cellular membrane[155, 156]. Meanwhile, the unknown angle between the direction of the applied external force (the tip moving direction) and the direction of the resistance force (the tangential direction of the interface between the adhesive colloid/cell and the substrate) cause some difficulty in evaluate the adhesion strength.

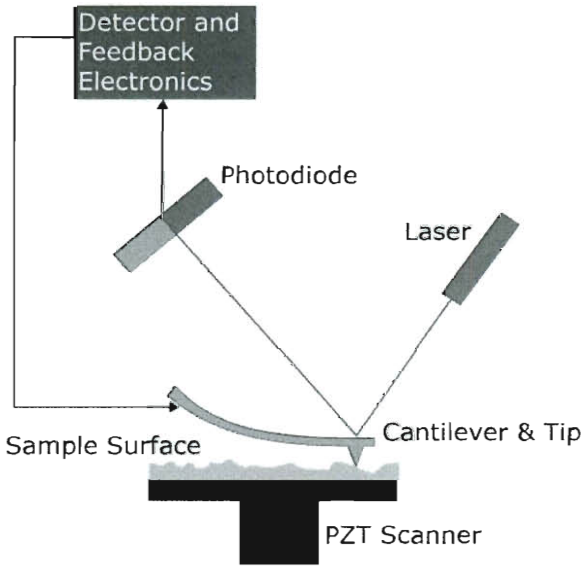

Figure 2. 9. Schematic of AFM operation (wiki)

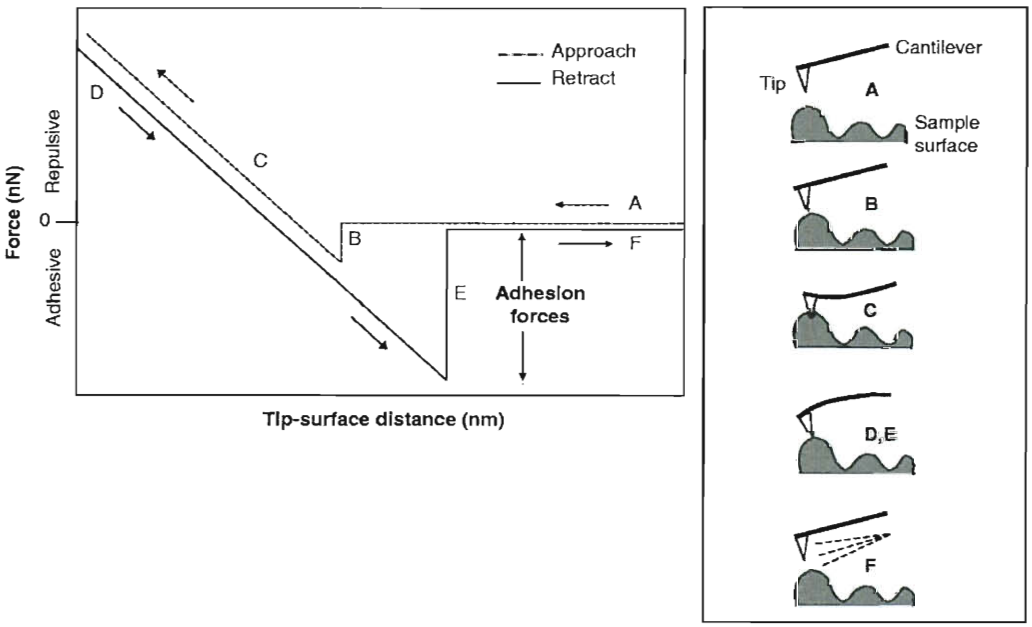

Figure 2. 10.Force-distance curve[157]

Usually colloid or bacterial cell can be attached onto the cantilever tip to make colloidal/bacterial probes and the detachment force of the colloid/cell (either in ambient condition or in a medium) that has adhered to a surface from the surface can be measured.

2.5.3 Parallel-Plate Flow Chambers (PPFC)

Method that involved parallel-plate flow chambers[158-160] in which a pump provides steady-state laminar fluid flow containing colloids/bacteria has been adopted to study the colloidal/bacterial adhesion phenomena under well defined hydrodynamic condition (Figure 2.11.). There are round shaped parallel-plate flow chamber and rectangular shaped parallel-plate flow chamber.

Typically, the suspension enters from one side of the chamber and leaves from an opposite side. There is a groove in the upper deck where the sample investigated can snuggly fit into. Colloidal/bacterial adhesion is viewed with an inverted epifluorescence microscope. Within the chamber flow channel, fluid flow creates shear stress (τ) at the channel wall and a typical equation describing this relationship as a function of flow rate, Q and channel height, h, can be derived from the Navier-Stokes and continuity equations:

$$\tau = \frac{6Q\mu}{wh^2} \qquad (2.18)$$

in which μ is the dynamic viscosity, and w is the width of the channel. The shear stresses exerted on the cells are assumed approximately equal to the channel wall shear stresses as the height of cell size is about two orders of magnitude less than the height of the channel[161].

This apparatus has been widely used because flow within the flow channel can be described mathematically with relative ease[162] and also it allows a global or probabilistic measurement of colloidal/bacterial adhesion strength[163]. However, special attention should be paid when micro- or nano-patterned surface is used for

turbulent flows are easily induced by the roughness, which makes the use of equation 2.16 restricted.

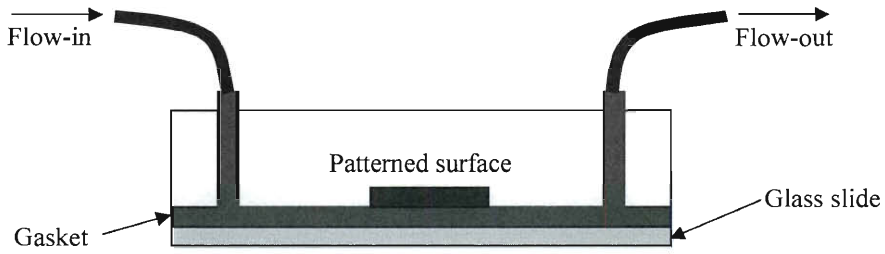

Figure 2. 11. Schematic of a typical rectangular parallel-plate flow chamber (cross-section)

2.5.4 Radial Stagnation Point Flow (RSPF) Systems

Radial stagnation point flow (RSPF) system has currently been used for the experiment for bacterial adhesion with the verification of DLVO theory. It is a well-characterized experimental system and is useful for visualizing the deposition of individual bacteria on the uniform charge, flat quartz surface[164, 165]. The deposition of bacteria on the surface was usually observed and estimated through an inverted microscope and recorded at regular intervals (10 s or 20 s) with a digital camera. It provides quantitative measurement of the strength of adhesion and kinetics of detachment for model systems which mimic the physiological and bioengineered systems.

Many bacterial strains have been used for the RSPF experiments, including: (1) *Cryptosproudium parvum oocysts*[166], having 3.7 μm equivalent spherical diameter;

(2) *Escherichia coli*[167, 168], having 1.7 μm equivalent spherical diameter; (3) *Psuedomonas Aeruginosa*[164, 165, 169, 170], having 1.24 μm equivalent spherical diameter.

Typical flow field at the stagnation point flow can be shown in Figure 2.12.

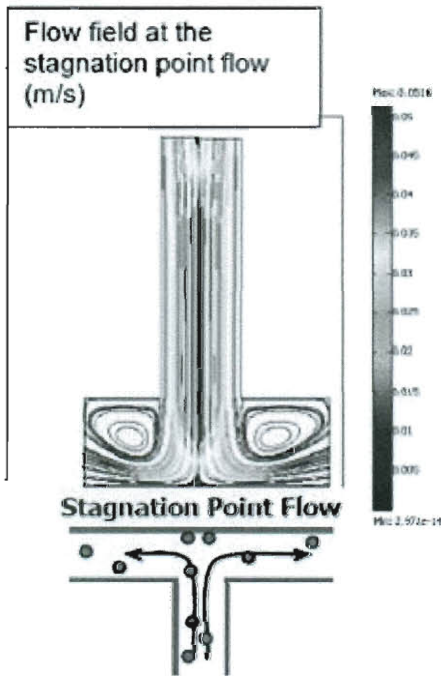

Figure 2. 12.Typical flow field at the RSPF system
(http://www.yale.edu/env/alexis_folder/alexis_research_2b.jpg)

Transport of bacteria from bulk liquid to surfaces strongly depends on the hydrodynamics of the system studied. With the PPFC and RSPF systems, adhesion can be measured in situ, which avoids uncontrolled effects of transfer of substrata through the air-liquid interface[171].

Some other methods, such as radial flow chamber[172] which allows direct in situ observation of adhesion and rotating disk system[173] which does not allow direct observation of the adhesion process have also been adopted.

2.6 Summary and potential

The effect of surface topography on bacterial adhesion reported from previous experimental studies has been controversial; and for most cases, random surface roughness or not so well controlled surface topography has been used.

Benefited from the development of micro- and nano-fabrication techniques, the availability of substrata with uniform and well defined surface topography have facilitated a systematic investigation into the role of substratum topography on bacterial adhesion, as well as the subsequent impact, like the physiology of bacterial cell. These studies have offered new insights into previous conclusions as to the physicochemical effect and biological response of bacteria to surface topography.

Inspired from the smartness of nature, more and more efforts have been made toward achieving these amazing behaviors, like lotus effect manually. And certain success has been made.

Further knowledge of the adhesion behavior on patterned surface with different topographies as well as the new development of newly designed surfaces will give clue to and enhance their industrial application in a tremendously wide areas, like water treatment membranes, medical devices etc.

3. Materials and Methods

3.1 Taro leaves

Taro (*Colocasia esculenta*) leaves were collected on Rice University campus. They were washed with DI water for five times. 1cm×1cm samples from the young, fully developed leaves with few veins were cut and attached to a small piece of glass side with double side tape. The samples were freshly prepared before experiments.

3.2 Design & Fabrication of Surface Patterns

*The fabrication of the micro-patterns was done by Dr. Lou's group part of the collaboration.

3.2.1Micro-Pattern

Silicon wafer substrates (500 ± 25 μm thickness; 100 mm diameter, (111) orientation) polished on one side were obtained from Addison Engineering, Inc. (San Jose, CA). For most experiments, the wafer substrates were typically cut down to smaller chips ~0.8 cm × 1.2 cm in size using a diamond-tipped scribe. Piranha clean was done at 110 to 130 degree C for 60 minutes to remove organic contaminations followed by drying with N_2. Using standard photolithography methods, arrays of patterns with different dimensions were manufactured on a single silicon chip. The cleaned chips were baked at 150 ℃ for 10 to 15 minutes. Two drops of S1813 photoresist were then spin-coated on the chips at 5000 RPM. After deploying a Mask Aligner (Suss Mask Aligner MJB4) to expose the chips, develop 319 was

subsequently used to remove the residual photoresist. The residual solution on the chips was blown dry. A chrome film of several micrometers in thickness was sputtered on the chips (CRC-150 Sputter Coater). The chrome coated chips were then boiled in Remover 1165 at 100 °C for 60 minutes. A standard Reactive Ion Etch (Minilock-Phantom III Trion RIE) procedure was employed to etch the chips to obtain topographic features of 2 to 3 μm in height.

Micro-patterned surfaces with a range of pillar sizes and spacings were designed to investigate how pattern dimensions affect the particle adhesion and distribution on the surface. Cuboid shaped pillar or pit was chosen for its easiness in fabrication.

After a series of preliminary experiments using micro-patterns of a wide range of dimensions, two arrays of micropatterns were fabricated to determine the effects of pillar size and spacing, respectively: (a) a series of patterns with fixed pillar spacing (5 μm) and varying pillar sizes from 5 μm to 40 μm; (b) a series of patterns with fixed pillar size (5 μm) and varying spacing from 5 μm to 40 μm. Each pattern covered an area of 1 mm ×1 mm and separated by a 0.3 mm wide gap. Figure 3.1 shows the schematic layout of the pattern. Control surfaces were etched smooth silicon wafer.

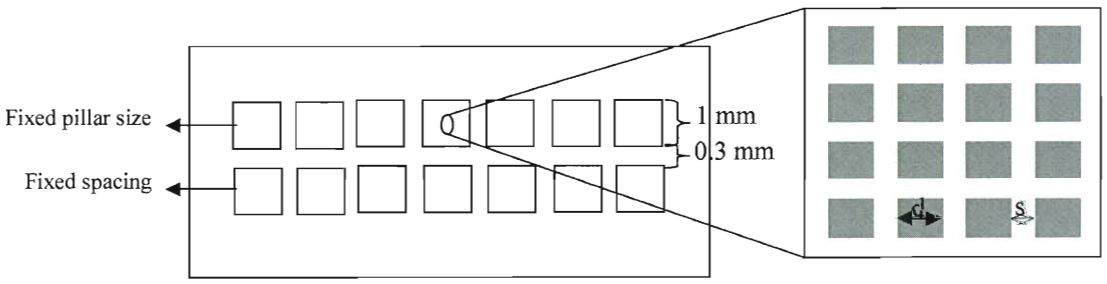

Figure 3. 1. Schematic layout of the patterned surface

The dimensions (pillar size, spacing between pillars and height of pillars) of all

patterns tested are listed in Table 3.1.

Table 3. 1. Dimensions of the two series of micro-patterns

Height (μm)	Spacing (μm)	Diameter (μm)
2~3	5	5
2~3	5	6
2~3	5	7
2~3	5	11
2~3	5	12
2~3	5	20
2~3	5	40

Height (μm)	Diameter (μm)	Spacing (μm
2~3	5	5
2~3	5	6
2~3	5	7
2~3	5	11
2~3	5	12
2~3	5	20
2~3	5	40

3.3 Direct visualization of colloidal/bacterial adhesion on natural and engineered surfaces

3.3.1 Particles used in the study

Carboxylate modified latex (CML) particles. Carboxylate modified latex (IDC, Eugene, OR, 4% solids) particles with a diameter of 4 or 6 μm were used in the study. The size of the particle was verified in the background solution used in the adhesion experiment (100 mM, NaCl, pH4) using an electrical sensing zone device (Multisizer 3, Beckman Coulter Inc., Miami, FL) with a 30-μm diameter aperture.

Carboxyl modified fluorescent microspheres. For better visualization, carboxylate

modified poly (styrene-co-acrylic acid) (PSAA) microspheres were also used. Fluorescence microspheres (1.0% solids, Phosphorex, Inc, Fall River, MA) of 4 μm in diameter were used in adhesion experiments with taro leaves, while those of 6 μm were used in experiments with micro-patterned surfaces. Over 99 wt% of the microsphere is PSAA with styrene being the predominant monomer unit. There is approximately 1% fluorescent dye inside the polymer microspheres. The excitation wavelength for the particles is 480 nm and the emission wavelength is 509 nm. The density of the carboxyl function groups is 6.02×10^7/sphere and stock suspension concentration is 8.4×10^7/ml.

Immediately before each experiment, the stock suspension of the microspheres was sonicated for 20 min in a sonicating bath immediately to achieve uniform dispersion of the microspheres in the suspension. Then, 37.5 μL of the stock suspension was added into 5 mL 100mM NaCl with pH adjusted to 4 using HCl to obtain a microsphere suspension with a number concentration of ~10^7/mL.

Surface zeta-potential of the fluorescent microspheres was characterized by electrophoretic mobility measurement using a Zetasizer Nano ZS (Malvern Instruments, Westborough, MA). Under the condition in which the adhesion experiments were performed, the microspheres had a slight negative surface zeta potential. This low zeta potential suggests weak electrostatic repulsion and consequently favorable particle adhesion on a negatively charged surface.

Preliminary experiments showed that the adhesion results from CML particles and fluorescently labeled PSAA microspheres with the same size were comparable.

Test bacteria. A common biofilm forming bacterial strain *Pseudomonas aeruginosa* (ATCC 700829) was used in this study. *P. aeruginosa* was cultured in the LB medium at 37 °C. The growth curve (Figure 3.2) showed that *P. aeruginosa* was in the exponential growth phase between 10 h and 40 h. Therefore, *P. aeruginosa* cells were harvested after 23 hrs of incubation. The cells were then washed three times with PBS buffer (8g NaCl, 0.2g KCl, 1.44g Na_2HPO_4, 0.24g KH_2PO_4 in 1L DI water, pH7.4) and used immediately in the adhesion experiments.

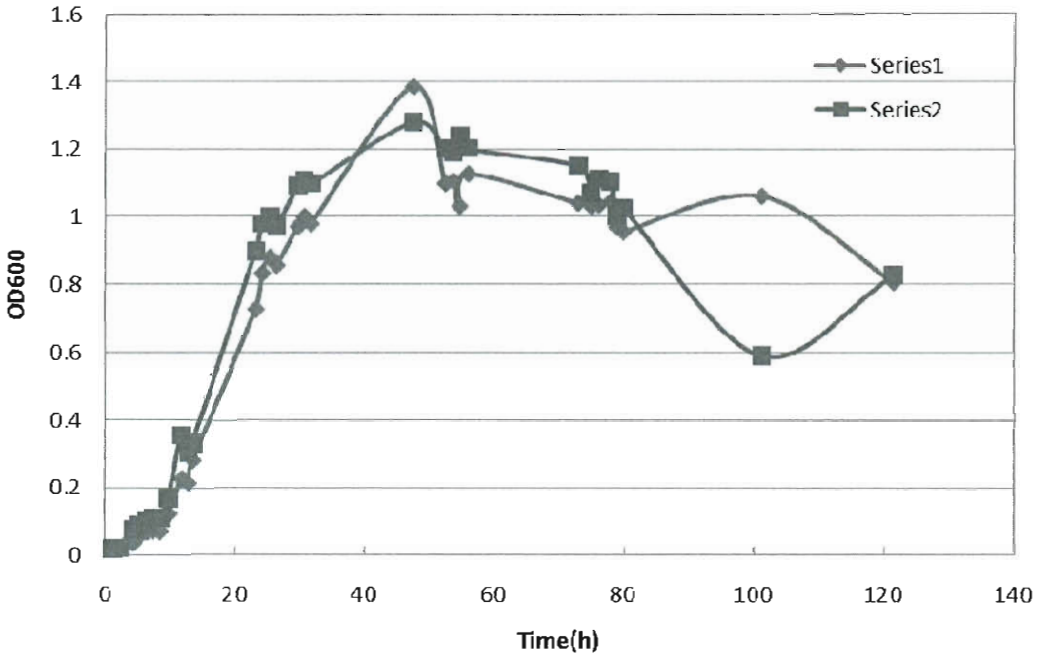

Figure3. 2. *Pseudomonas aeruginosa* growth curve obtained in LB at 37 °C (Series 1 and 2 are parallel experiments)

3.3.2 Particle/bacterial Adhesion Assays

Preparation of sample surfaces.

Fresh taro leaves were used immediately after collection. The leaves were washed five times with DI water. The a piece of the leaf sample was cut (1cm×1cm) from the middle section of the leaf and mounted onto a 2.5cm×2.5cm glass with double sided tape.

The micropatterned silicon wafers as well as the smooth control surface were cleaned according to the following protocol. Samples were fist soaked in 2% Extran MA02 solution (EM science, Gibbstown, NJ) for 2h, and rinsed with ethanol followed by deionized water. Next they were sonicated in a 2% RBS 35 detergent solution for 20 min in a sonication bath and rinsed again with ethanol and deionized water. The samples were then soaked in a NOCHROMIX solution (GODAX Laboratories, Inc.) for 24 h and thoroughly rinsed with deionized water. The surfaces were dried with ultrapure nitrogen filtered through a Whatman HEPA-CAP^{TM} filter.

Adhesion experiments

A six-well plate was cleaned and dried with particle-free ultrapure nitrogen. Sample surfaces were placed side by side in one cell of 30 mm in diameter on the six-well plate. The prepared particle/bacterial suspension was then added into the wells. The plate was then put on an orbital shaker table (VWR OS-500, West Chester, PA) and incubated at room temperature for 30 min at 50 rpm. For experiments using fluorescent microspheres, the plate was wrapped in aluminum foil to avoid photo bleaching. At the end of the incubation, the samples were rinsed 5 times with NaCl background solution (for particle) or PBS (for bacterial adhesion) to remove the residual and loosely attached particles/bacteria. Experiments were repeated twice.

Enumeration of adhered particles/bacteria by optical or epifluorescence microscopy.

CML particles. When CML particles were used in the experiment as the model colloids, the testing surface (taro leaf and patterned surface) were rinsed gently with the background solution (100mM NaCl with pH adjusted to 4 using HCl) three times at the end of 30 min incubation. The rinsing was done by replacing the residual particle suspension with particle-free background solution without taking the sample surface out of the suspension in order to avoid disturbance by the air-liquid-solid interface, a common but often overlooked problem when the sample surface was taken out of the suspension for rinsing. A glass cover slip was then carefully put on the surface, leaving a thin film of background solution in between. Then the samples were visualized using an optical microscope (Z16 APO, LEICA; Qimaging MicroPublisher 3.3 RTV Camera) to observe the distribution of particles on the sample surface.

Carboxyl Modified Fluorescent microspheres and bacteria. At the end of the 30 min incubation, the taro leaf or patterned surface samples were rinsed gently with the background solution (100mM NaCl with pH adjusted to 4 using HCl in fluorescent microsphere adhesion experiments and PBS in bacterial adhesion experiments) three times (rinsing method same as for CML particles). Bacteria on the leaf, specifically the nucleic acids were stained with 1 μg/mL 4', 6-diamidina-2-henylidole (DAPI) for 5 min and then rinsed. Taro leaf coupons were photographed with an upright Axioplan 2 epifluorescence microscope (Carl Zeiss, Oberkochen, Germany). Images were acquired with a CoolSnap HQ camera (Photometrics, Tucson, Ariz.) controlled by

Metamorph 7 imaging software (Molecular Devices Corporation, Sunnyvale, CA). DAPI displayed background fluorescence on the leaves that had not been exposed to bacteria; deconvolution procedure was carried out using the software after the images were obtained in order to get a better color contrast.

Quantification of Adhered Particles/bacteria. To quantify the number of adhered colloidal particles on the surface, five images were taken for each sample. The images were then analyzed using the ImageJ software[174] to determine the average number of particles attached per unit area.

3.4 Sample surface characterization

3.4.1 SEM imaging

To examine the surface structure of the taro leaf, 1cm×1cm samples were cut from the young, fully developed leaves at locations with few veins were cleaned by DI water, air-dried and then affixed to aluminum SEM sample stubs using double-sided adhesive carbon tapes. The specimens were then sputter coated with gold and examined in a high resolution field emission scanning electron microscope (FEI Quanta 400 ESEM FEG)

3.4.2 XPS analysis

Chemical element analyses of the taro leaf and the patterned as well as smooth silicon wafers were performed using a PHI Quantera X-ray photoelectron spectroscopy (XPS).

3.4.3 Profilometry

Pillar structured micro-patterns on silicon wafers were characterized with a Veeco DekTak 6M stylus profilometer to examine the 3-D pattern structure and to accurately measure pillar height.

3.5 Adhesion force measurement

The adhesion force on the taro leaf or micro-patterned silicon surfaces was measured by atomic force microscopy (AFM). AFM adhesion force mapping was performed in Dr. Jun Lou's lab as a part of the collaborative project. The experimental methods and results are included in this thesis for completeness of the discussion.

3.5. 1. Measurement of adhesion forces on a Taro Leaf (*Colocasia esculenta*)

A piece of fresh Taro Leaf was cleaned, cut and attached to an AFM sample holder using double sided tape. The sample was then mounted in a fluid cell where it was immersed in the background solution used in the adhesion experiments and loaded into a Pico-plus AFM (Agilent AFMs, Tempe, Arizona). A silicon AFM probe (PPP-NCH-W, NanoSensors, Neuchatel, Switzerland) with spring constant 0.44 N/m was used for the measurement.

A scan was first performed over a 10 μm by 10 μm area of the leaf sample to map out the topography of the leaf surface. Then two surface photovoltage spectra scans were performed over a 1 μm by 1 μm area, one on top of a papilla and the other over a ridge to measure the adhesion force over each area. Each SPS scan consisted of

1024 force vs. displacement curves in a 32 by 32 grid. The adhesion force over a point was calculated from the difference between the zero deflection point and the minimum deflection recorded in the force vs. displacement curve at that point.

3.5.2. Measurement of adhesion forces on engineered patterned surfaces

The adhesion force between a CML particle and the patterned as well as the smooth silicon surfaces was measured using a colloid probe. The colloid probe was prepared by attaching a CML particle of 6 μm in diameter to the end of a tipless AFM probe with a 24-hour epoxy using a micromanipulator. The colloid probe was stored in dark at 4 °C when not used. An optical microscopic image of a colloidal probe is shown in Figure 3.3(a). The surface image (Figure 3.3(b)) of the colloid probe was obtained by scanning calibration surface containing sharp arrays using the probe.

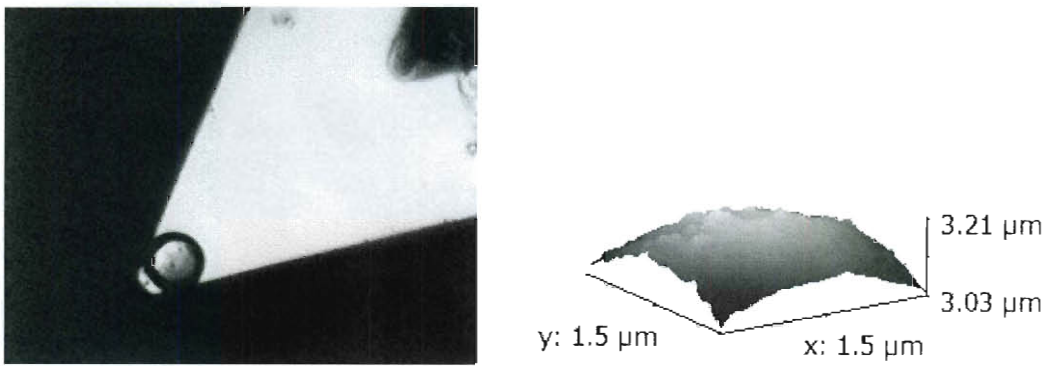

(a) (b)

Figure3. 3. (a) Microscopic image of the CML colloid probe and (b) AFM image of the colloid probe tip

Force vs. distance measurements were performed on different micro-patterns as well as the smooth control surfaces. All measurements were performed the same

background solution (100 mM NaCl with pH adjusted to 4 using HCl) as that used in the adhesion experiments. A robust procedure was developed in this study to construct an adhesion force map consisting of 1024 force-distance spectroscopy curves in each scan to characterize adhesion characteristics of the samples with proper statistical treatments.

4. Nanostructure on Taro Leaves Resists Fouling by Colloids and Bacteria under Submerged Conditions[1]

Jianwei Ma[1], Yuekai Sun[2], Karla Gleichauf[1], Jun Lou[2], and Qilin Li[1]
1. Dept. of Civil and Environmental engineering, Rice University, Houston, Texas 77005
2. Dept. of Mechanical Engineering and Materials Science, Rice University, Houston, Texas 77005

4.1 Abstract

The anti-fouling and self-cleaning properties of plants such as *Nelumbo nucifera* and *Colocasia esculenta* have been attributed to the superhydrophobicity resulting from the hierarchical surface structure of the leaf and the air bubbles trapped between the nano-sized epicuticular wax crystals. The reported study showed that the nano-sized structures on the papilla of *Colocasia esculenta* or taro epidermal cells were also highly resistant to particle and bacterial adhesion under submerged conditions when the surface was completely wetted. Adhesion force measurements using atomic force microscopy revealed that the adhesion force on top of the papilla was markedly lower than the rest of the leaf surface. The decreased adhesion force and the resistance to particle and bacterial adhesion were attributed to the dense nano-structure found on the epidermal papilla.

---

[1] Manuscript to be submitted to *Langmuir*.
[2] Jianwei Ma's contribution to the paper includes: Taro leaf surface characterization; taro leaf wetting; adhesion of fluorescent microsphere on taro leaf; adhesion of *Psudomonas Aeruginosa* on taro leaf.

4.2 Introduction

Although the phenomenon of water repellency property exhibited by lotus leaves and other plant leaves has been noticed for a long time, it was not until 1997 that the surface structure of lotus leaves was found to have significant impact on the observed phenomena[100, 101]. And since then the lotus leaf effect and the resulting self-cleaning and anti-fouling properties have been a topic of intensive research. However, it is necessary to note that although it is called "lotus effect", there are many other plant leaves which have similar antifouling or self-cleaning surfaces with different unique surface structures, such as taro leaves. There are numerous potential applications for lotus effect in different areas, such as self-cleaning paint, clothes, windows, chips, biorepellent coating, antistiction coating and bioMEMS etc[175].

The lotus effect is believed to be caused by a combination of chemical and physical properties. The chemical effect is mainly due to presence of wax crystalloids through out the surface, which makes the surface hydrophobic; the contribution of physical properties originates from its surface topology, which when combined with the chemical attributes, makes the surface superhydrophobic[176-179]. The chemical effect has been studied widely and conclusively to be a factor determining the lotus effect behavior[180, 181]. Barthlott and Neinhuis[100] for the first time revealed that the unique surface topographic structure of these leaves reduced particle adhesion, and water repellency was the keystone in the self-cleaning mechanism of many biological surfaces. Following them, much research has conducted to further investigate the topography impact on lotus effect[182].

Although the role of surface topology in superhydrophobic and self-cleaning surfaces is well recognized, studies reported so far were limited to applications where the surface is not completely wet and the nano-structures on the surface cause superhydrophobicity by trapping fine air bubbles. Superhydrophobicity is believed to be the basis for the self-cleaning. It has been reported that the superhydrophobicity property of lotus leaves disappear after they are immersed under certain hydraulic pressure for some time[183]. The mechanism is believed to be extrusion of the tiny air bubbles trapped in the nano-structure. However, whether the lotus effect surfaces could still be self-cleaning or fouling-resistant when completely wetted, e.g., under longer-term submersion in water is unknown. The objective of this study is to investigate the impact of surface topographic structure of a lotus effect surface on particle and bacterial adhesion under completely submerged conditions.

In this study, we tested adhesion of biological (*P. aeruginosa*) and non-biological (carboxyl modified poly (styrene-co-acrylic acid) microspheres) particles on the surface of taro leaves under conditions where the leaf surface was completely wetted or non-wet. The results confirmed that the superhydrophobicity caused by fine air bubbles trapped between nano-sized surface features play an important role in resisting particle/bacterial adhesion. More importantly, the study showed that even when the taro leaf surface was completely wet, the nano-structures on taro leaf surface were resistant to adhesion of both bacteria and abiotic particles. To our knowledge, this is the first study investigating the "under-water" fouling behavior of natural surfaces that are known to be self-cleaning or anti-fouling. Our findings suggest that

properly designed surface nano-structures have great potential for particle and bio-fouling control in under-water applications.

4.3 Experimental Section

Materials

Young, fully developed *Colocasia esculenta* (taro) leaves were collected from Rice University campus and used immediately after collection. The leaves were thoroughly rinsed with DI water before use. Samples of 1 cm $\times$ 1 cm in size were cut from the middle section each leaf, avoiding areas with large veins. For adhesion experiments, the samples were mounted onto a 2.5 cm $\times$ 2.5 cm microscope glass slide with double sided tape.

Carboxylate modified poly (styrene-co-acrylic acid) (PSAA) microsphere labeled with green fluorescence were obtained from Phosphorex, Inc (Fall River, MA). According to the manufacturer, the particles were 4 μm in diameter with a carboxyl group density of 6.02×10^7/sphere. Immediately before the particle adhesion experiments, the stock suspension of the PSAA microspheres (8.4×10^7/ml) was sonicated for 20 min in a sonicating bath to ensure uniform dispersion. 37.5 μL stock fluorescent microsphere solution was added into 5 mL background solution (100 mM NaCl with pH adjusted to 4 using HCl) to obtain a microsphere suspension with a number concentration of ~10^7/mL.

pseudomonas aeruginosa (ATCC 700829), a known biofilm forming bacterium, was used to study bacterial adhesion on the taro leaf.

Reagent-grade 190 proof ethanol (95%) was obtained from DECON Labs, Inc (King of Prussia, PA).

Reagent-grade NaCl was obtained from Fisher Scientific (Pittsburg, PA).

Hydrochloric Acid (GR, ACS Grade, 37%, Darmstadt, Germany)

All solutions and suspensions were prepared using ultrapure water ($\geqslant$18.1 mega Ω -cm) generated by an E-Pure system (Barnstead, VWR, Batavia, IL).

Characterization of taro leaf surface

SEM imaging. To examine the leaf surface structure, 1cm×1cm leaf samples were air-dried and affixed to aluminum stubs with double-sided adhesive carbon tapes. The specimens were then sputter coated with gold (CrC-150 Sputtering System, TORR International, New Winsor, NY) and examined with a high resolution field emission scanning electron microscope (FEI Quanta 400 ESEM FEG, Hillsboro, Oregon)

Pretreatment of the taro leaf

Surface conditioning. For experiments performed without pre-wetting of the taro leaf surface, the leaf samples were soaked in the background solution used in the adhesion experiments for three days in dark at 4 °C to allow chemical equilibrium.

Surface wetting treatment. Because of its superhydrophobicity, it was very difficult to wet the taro leaf surface. Three different wetting methods were tested and described below.

Soaking treatment. Soaking under a sufficient hydrostatic pressure has been reported to wet the lotus leaf[183]. In our study, the taro leaf sample was mounted at the bottom of a graduated cylinder, in which the background solution (100mM NaCl at

pH4 or PBS) was added to amount a water column height of 45 cm for three days.

Water vapor condensation. Another method that has been shown to wet the lotus leaf is through water vapor condensation. A similar method was tested in our study using the set up shown in Figure 4.1. A taro leaf sample was mounted face down covering the opening of a 1000 mL beaker flask. The beaker flask was filled with 500 mL DI water with a 14 cm distance between the water surface and the leaf sample. The water in the beaker was then heated to a target temperature (60 °C, 70 °C, 80 °C or 85 °C) for 20 min. Ice was placed on top of the plate to aid the condensation of the water vapor as well as to keep the leaf from being overheated. A previous study reported that temperatures above 90 °C could damage the structure on the structure of the lotus leaf[184].

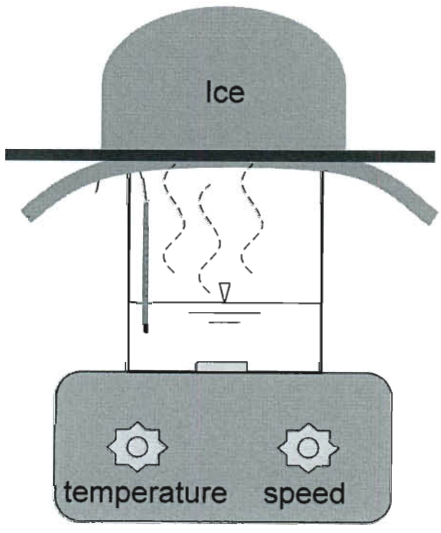

Figure 4. 1. Schematic of the experimental setup for the water vapor condensation method to wet the taro leaf surface

Ethanol Wetting. Because of its low surface tension, ethanol was used to wet the leaf surface in order to remove the air-bubbles trapped in the nano-structure on the taro leaf surface. Several drops of ethanol were added onto the taro leaf surface and finally the drops of ethanol spread throughout the surface to form a thin film; water can spread on this surface.

Particle adhesion experiments.

Particle adhesion experiments were performed with the PSAA fluorescent microspheres in 100 mM NaCl with pH adjusted to 4 with HCl. This solution condition was chosen to minimize the electrostatic repulsion between the PSAA particles and the taro leaf surface in order to create a favorable condition for particle adhesion. The number concentration of the PSAA particles in the suspension was $\sim 10^7$/mL.

A six-well plate was cleaned thoroughly and dried with particle-free ultrapure nitrogen. The properly leaf samples were mounted on the bottom of each well of 30 mm in diameter. The prepared PSAA particle suspension (5 mL) was then added into each well. The plate was then wrapped in aluminum foil and put on an orbital shaker table (VWR OS-500, West Chester, PA) and incubated at 20 ºC for 30 min at 50 rpm. At the end of the incubation, the suspension was pipetted out leaving a thin liquid layer above the surface; the samples were rinsed 5 times gently with the background solution and imaged using an upright Axioplan 2 epifluorescence microscope (Carl Zeiss, Oberkochen, Germany) for quantitative analysis of the particles adhered.

Bacterial adhesion experiments.

P. aeruginosa cells were cultured in the LB medium at 37 °C. Cells were harvested after 23 hrs of incubation (mid-exponential growth phase) and washed three times with PBS buffer. The washed cells were re-suspended in the PBS buffer to achieve a number concentration of ~2×10^7 CFU/mL. The cell suspension was then added into the wells of a six-well cell culture plate on the bottom of which the leaf samples were mounted. The plate was then put on an orbital shaker table (VWR OS-500, West Chester, PA) and incubated at 20 °C for 30 min at 50 rpm.

After incubation, the leaf samples were removed from the culture plate and rinsed three times gently with PBS buffer. The samples were then stained with 1 μg/mL 4', 6-diamidina-2-henylidole (DAPI) for 5 min and subsequently rinsed with PBS buffer for three times. The stained samples were mounted on a glass slide and imaged with an upright Axioplan 2 epifluorescence microscope (Carl Zeiss, Oberkochen, Germany). Images were acquired with a CoolSnap HQ camera (Photometrics, Tucson, Ariz.) controlled by the Metamorph 7 imaging software (Molecular Devices Corporation, Sunnyvale, CA). Because the stained samples displayed significant background fluorescence, an image deconvolution procedure was carried out to minimize interference from the background fluorescence.

Adhesion force mapping by atomic force microscopy (AFM)

The "stickiness" of the taro leaf surface was probed by performing adhesion force mapping using a Pico-plus AFM (Agilent AFMs, Tempe, Arizona). A 1 cm × 1 cm wetted leaf sample was fixed on an AFM sample holder using double sided tape.

The sample was then mounted in a fluid cell where it was immersed in the background solution used in the particle adhesion experiments. A silicon AFM probe (PPP-NCH-W, NanoSensors, Neuchatel, Switzerland) with spring constant 0.44 N/m was used for both surface imaging and the force measurement.

A scan was first performed over a 10 μm × 10 μm area of the leaf sample to map out the topography of the leaf surface. Then surface photovoltage spectra scans were performed over two 1 μm × 1 μm area, one on top of a papilla and the other over a ridge to measure the adhesion force over each area. Each SPS scan consisted of 1024 force vs. displacement curves in a 32 by 32 grid. The adhesion force over a point was calculated from the difference between the zero point deflection and the minimum deflection recorded in the force vs. displacement curve at that point.

4.4 Results and Discussion

4.4.1 Taro Leaf Surface Characterization

SEM images in Figure 4.2 show the surface structure of the taro leaf. The polygonal shaped epidermal cells from micro-scale "bumps" of 15 μm to 30 μm in diameter on the surface, with a papilla at the center of each cell. The surface of each cell was covered with nano-sized epicuticular wax crystals composed of aliphatic compounds[180]. These epicuticular wax crystals were believed to play an important role in the self-cleaning mechanism of lotus and taro leaves[181]. It is important to note, however, that the distribution of the nano-crystals was not uniform: the highest density was found on the papilla and the lowest on the edge of each cell.

XPS analyses performed at different locations on the same leaf sample resulted in almost identical survey spectra, suggesting no notable spatial variation of surface chemistry on the taro leaf. Figure 4.3 presents a representative XPS spectrum of the leaf surface. Elemental analysis shows 98.21% and 1.97% atom concentration of carbon and oxygen, respectively.

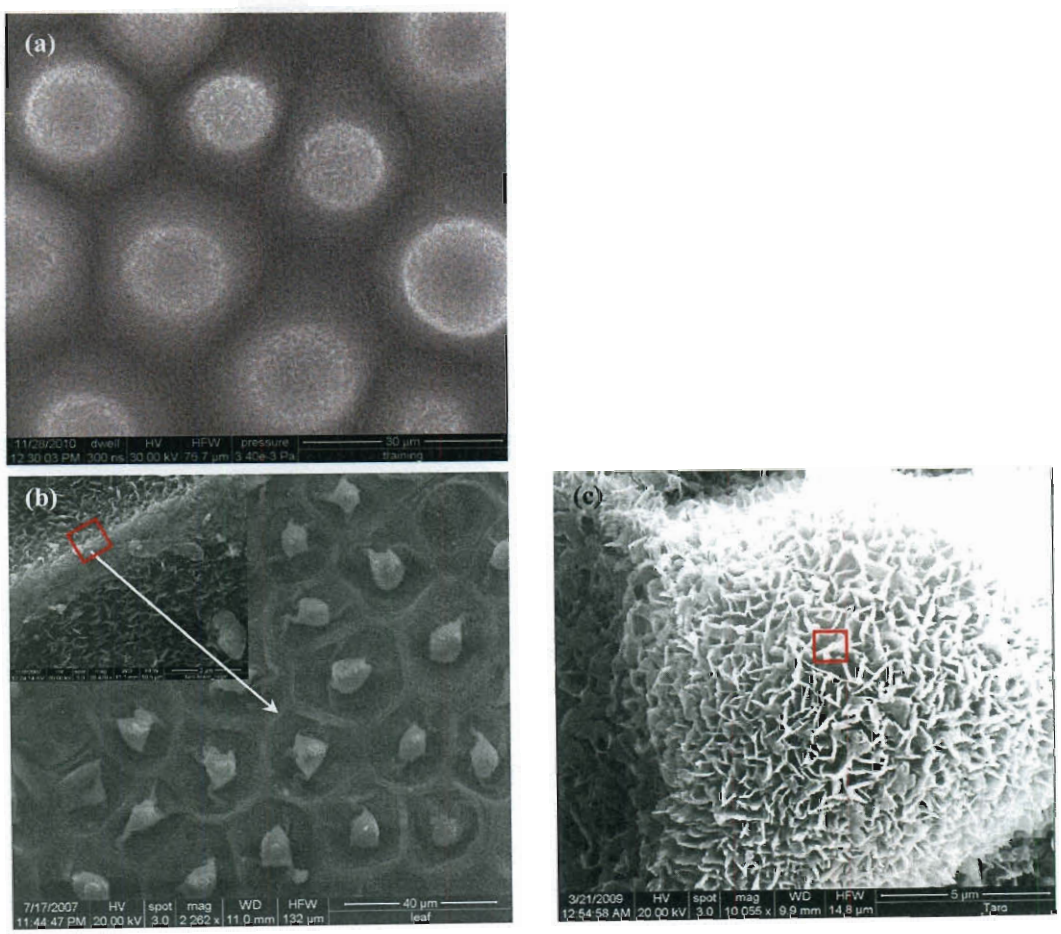

Figure 4. 2. Scanning electron micrographs of the taro leaf (a) throughout surface; (b) single micro-structure unit; (c) nano-structure on the center papilla (two red squares show where the AFM scanning was made)

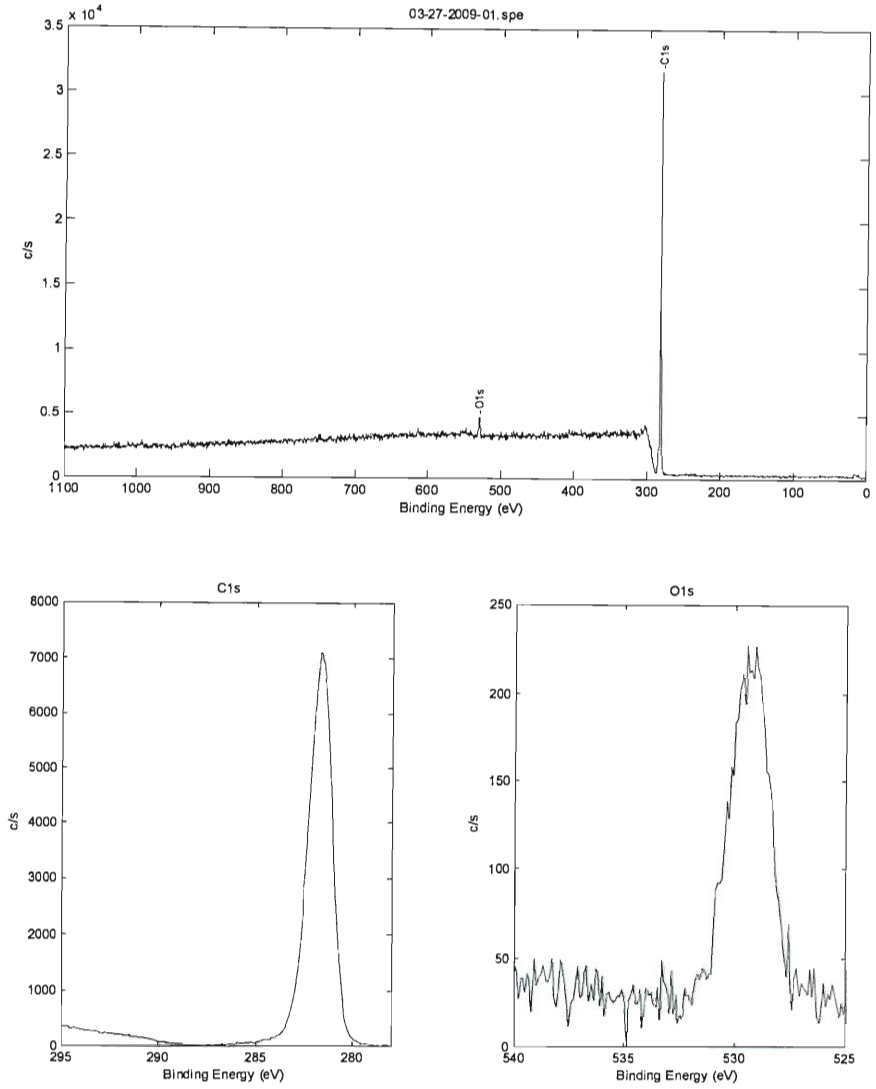

Figure 4. 3. XPS analysis for taro leaf surface (Atomic concentration: C1s[0.314] 98.21%; O1s[0.733]1.79%)

4.4.2 Taro Leaf Wetting

Neither soaking under hydrostatic pressure nor water vapor condensation was able to properly we the taro leaf surface. After three days of soaking under a hydrostatic pressure of 450 mm H_2O, a thin layer of air-bubble was still clearly visible

on the taro leaf surface and the surface was still superhydrophobic (Figure 4.4).

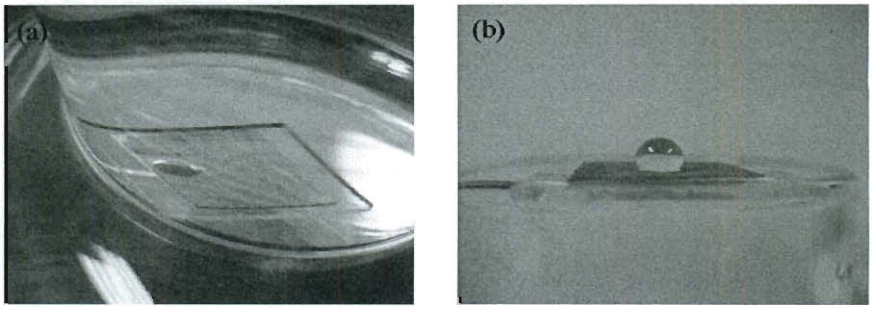

Figure 4. 4. Taro leaf surface after soaking under 450 mm H_2O for 3 days. (a) The taro leaf sample photographed on the bottom of the graduated cylinder; (b) A water bead formed on the taro leaf sample surface after three days of soaking treatment

Using the water vapor condensation method, the condensed water formed large drops after 20 min of treatment at 60 ºC, suggesting that the surface was not completely wet (Figure4.5 (a)). When treated at 70 ºC, part of the leaf surface was damaged as evidenced by the color change. On the damaged surface, water could spread as a thin film, but formed large drops in the rest of the surface (Figure4.5 (b)). Treatment at 80 and 85 ºC caused severe damage of the leaf (Figure4.5 (c) and (d)).

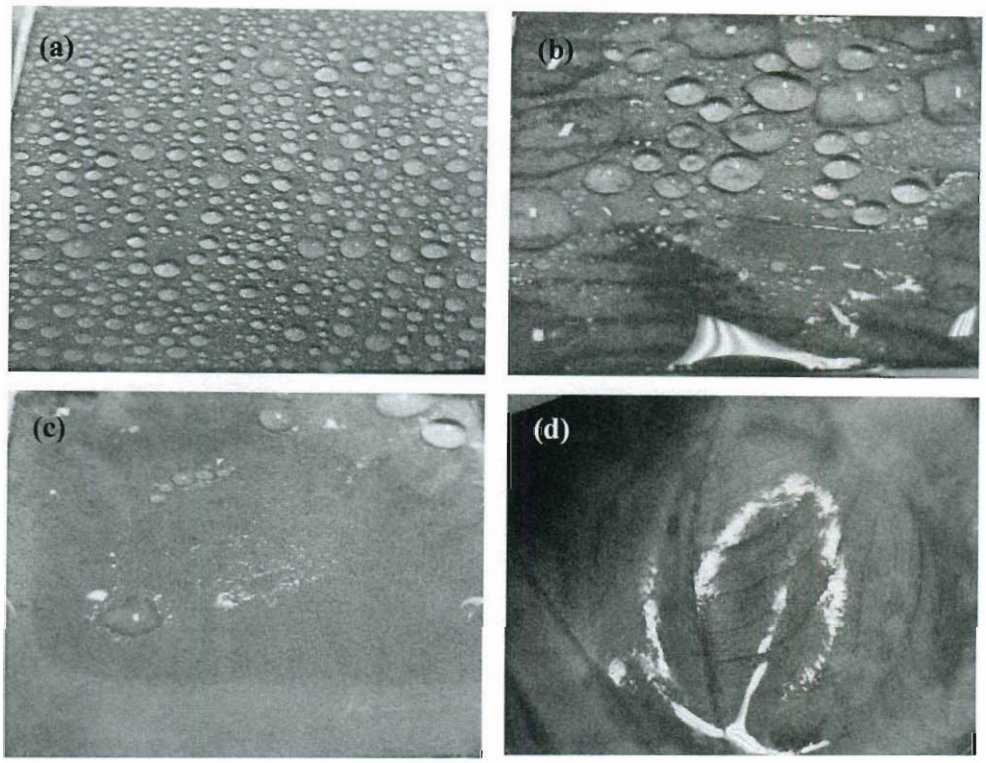

Figure 4. 5. Taro leaf after water vapor condensing with different temperatures (a) 60 °C; (b) 70 °C; (c) 80 °C; (d) 85 °C

Although the taro leaf still exhibited hydrophobicity after soaking in 50% ethanol, treatment with 190 proof ethanol (95%) was able to completely wet the leaf surface (Figure 4.6). Therefore, all adh6sion experiments of wetted leaf surface were performed using leaf samples treated by 95% ethanol.

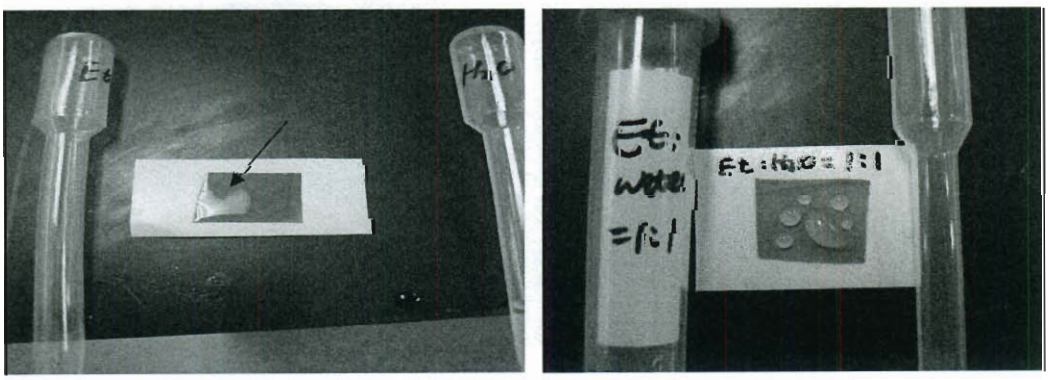

Figure 4. 6. Wet of taro leaf by (a) 95% ethanol; (b) EtOH:water (v/v)=1:1

4.4.3 Adhesion of PSAA microspheres

Few PSAA particles adhered to the taro leaf surface under the "non-wet" conditions, i.e., without ethanol treatment (Figure 4.7). This is consistent with the low fouling property of taro leaves as a result of the superhydrophobicity of the surface.

It has been hypothesized that fine air bubbles trapped between the nano-strutures on the leaf surface are responsible for the superhydrophobicity and therefore particle fouling resistance. It is interesting that the small number of particles that did adhere all adhered on the edge of epidermal cells, where the density of the nano-sized wax crystals is the lowest. Another observation was that no aggregates of particles were found on the non-wet leaf surface.

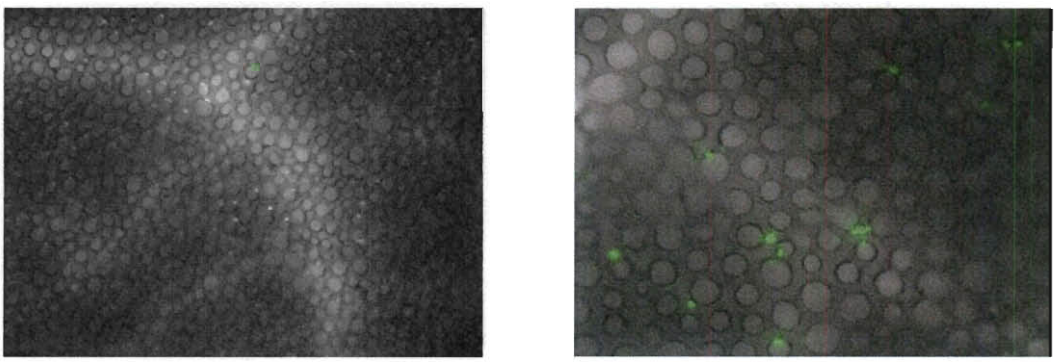

Figure 4. 7. Fluorescence microscope images of fluorescent microsphere adhesion on taro leaf (non-wet)

When the taro leaf surface was completely wet, i.e., no air bubbles trapped between the nano-structures, more PSAA particles adhered to the leaf surface compared to the non-wet surfaces, and some particle aggregates were found on the leaf surface (Figure 4.8). Such difference again demonstrates the importance of the

surface nano-structure and the resulting surface hydrophobicity in resisting particle fouling. However, despite the increased overall particle adhesion, the wetted leaf surface exhibited a particle distribution pattern similar to that observed with the non-wet surface: particles adhered only between the micro-sized epidermal cells, i.e., on the edge of each cell. This suggests that the dense nano-structures on taro leaf surface could resist particle adhesion under completely submerged conditions

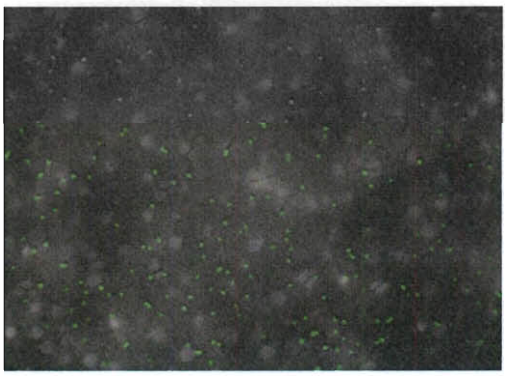

Figure 4. 8. Fluorescence microscope images of fluorescent microsphere adhesion on taro leaf (wet)

4.4.4 Adhesion of *Pseudomonas aeruginosa*

Similar to that observed with the PSAA particles, notably more *P. aeruginosa* cells adhered on the wetted leaf surface than the non-wet surface (Figure 4.9, Figure 4.10). Adhesion of *P. aeruginosa* was significantly higher than that of the PSAA particles under both wet and non-wet conditions. In addition, most *P. aeruginosa* cells were found linked together in the form of aggregates. Nevertheless, *P. aeruginosa* adhesion exhibited similar patterns as the PSAA microspheres on both wetted and non-wet taro leaf surfaces: *P. aeruginosa* cells adhered mostly on the edge of each epidermal cell unit of the taro leaf, displaying circular patterns throughout the test

surface. Considering that there is no notable variation in surface chemistry on the leaf surface, the spatial difference in *P. aeruginosa* adhesion is likely due to the difference in surface topology. The areas with denser nano-structures seemed to be highly resistant to *P. aeruginosa* adhesion.

These results show that surface nano-structure on the taro leaf surface can resist adhesion of both biological and non-biological particles, suggesting that the nano-sized surface features could significantly alter the physicochemical interactions between a bacterial cell or a colloidal particles and a rough surface. Because the same effect was observed under both wet and non-wet conditions, the observed particle/bacterial fouling resistance is considered independent of the superhydrophobicity of the taro leaf. This suggests that properly designed surface nanostructures may have anti-fouling properties in completely submerged conditions.

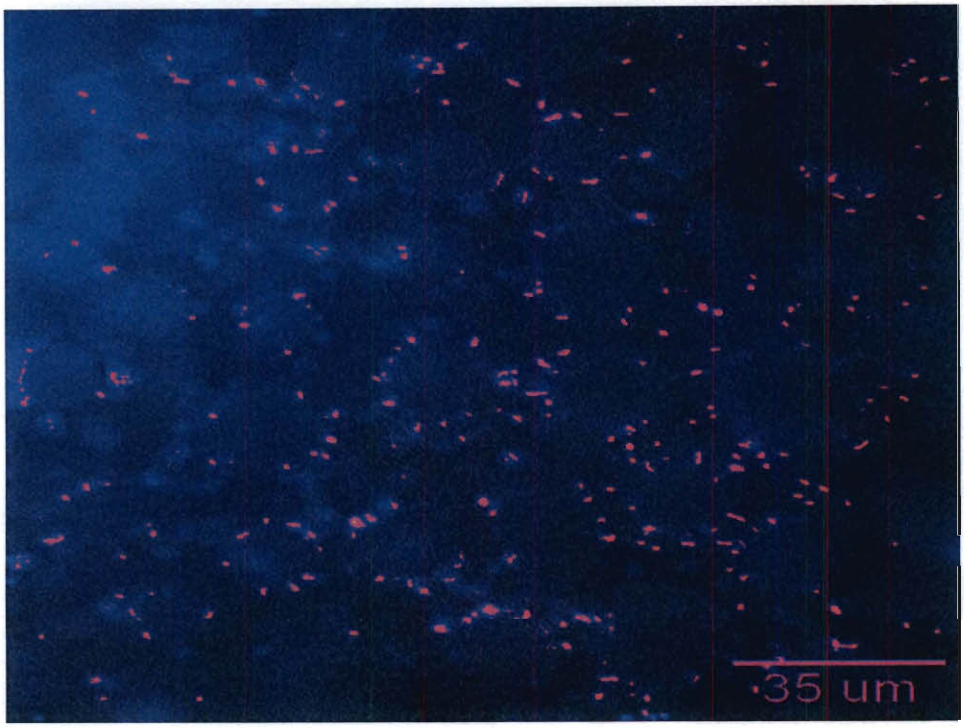

Figure 4. 9. Fluorescence microscope images of *Pseudomonas aeruginosa* adhesion on taro leaf (non-wet)

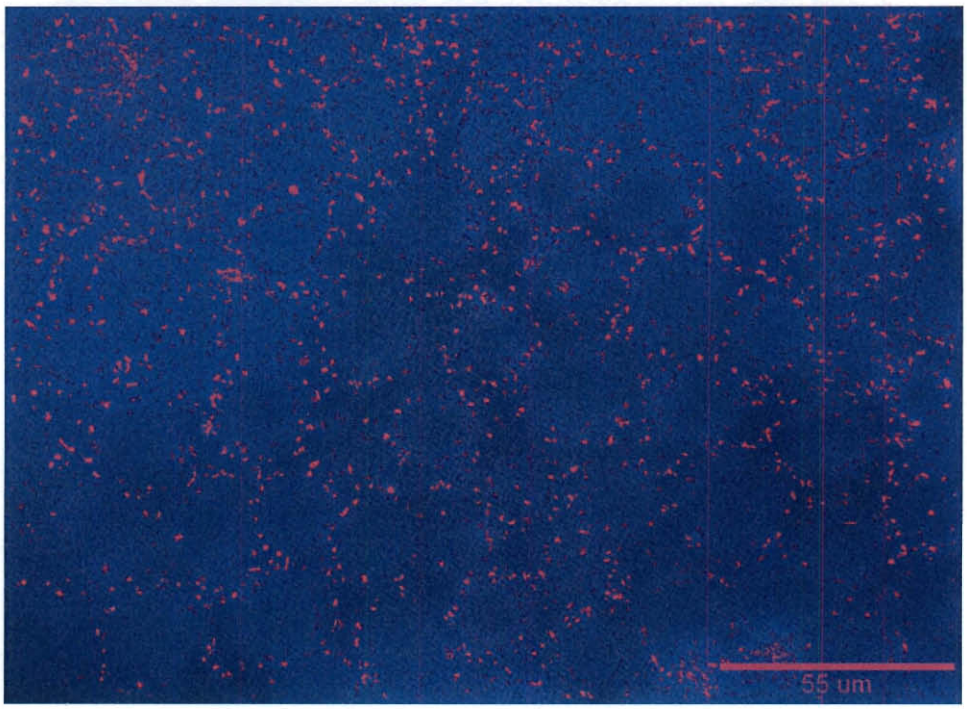

Figure 4. 10. Fluorescence microscope images of *Pseudomonas aeruginosa* adhesion on taro leaf (wet)

4.4.5 Adhesion forces mapping

In order to determine how the surface topography of the taro leaf affects its physicochemical interactions with a particle, atomic force microscopy was used to probe the spatial distribution of the adhesion force between an silicon AFM cantilever tip and the taro leaf surface.

Figure 4.11 shows the adhesion force maps obtained over two areas on the surface of a single leaf epidermal cell with the approximate locations where the measurements were made shown in Figure 4.2. The force maps show regions with distinct adhesiveness. The average adhesion force measured over the central papilla (17 nN) was only one third of that measured over the edge of the cell unit (~50 nN). The lowest adhesion was found between the edge and the central papilla, ~ 9 nN. Such distribution of adhesion forces correlates well with the observed adhesion pattern of PSAA particles or *P. aeruginosa* cells, i.e., adhesion occurred on the edge of the epidermal cell unit, where the measured adhesion force was the highest. Considering the similarity in surface chemistry over these areas, it is reasonable to hypothesize that the difference in adhesion force has to do with the density and distribution of the surface nano-structures.

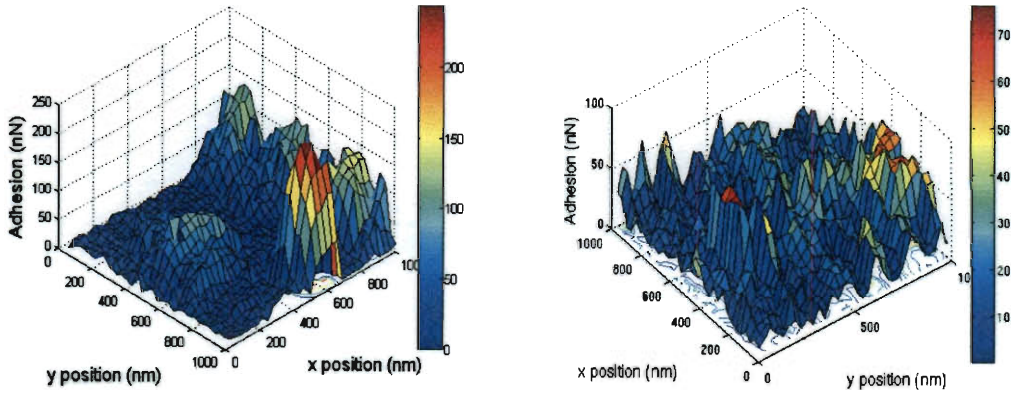

(a) (b)

Figure 4. 11. Adhesion force map (a) on the ridge (~50nN) and (b) on top of a papilla (~17nN)

It is noted that the forces measured are different from what experienced by the PSAA particle or the *P. aeruginosa* cell due to the difference in size, material and surface chemistry between the AFM cantilever tip and the PSAA particle or the *P. aeruginosa* cell. However, the measured adhesion force should correctly reflect the effect of the taro leaf surface topology.

4.5 Conclusion

Adhesion experiments using both biological (*P. aeruginosa*) and non-biological (carboxyl modified poly (styrene-co-acrylic acid) microspheres) particles showed that the nano-structures on taro leaf surface could resist particle/bacterial fouling under both wet and non-wet conditions. Although the anti-fouling property under no-wet conditions was believed to be the results of air bubbles trapped between the nano-structures, the fouling resistance observed under completely wet conditions is attributed to the reduced adhesion force on the area covered by dense nano-sized

surface features. This exciting discovery suggests that engineered surfaces with properly designed topographic structures could potentially prevent particle/biofouling in a wide range of under-water applications. This provides a novel, environmentally friendly approach to biofouling control, and industrial challenge with great economic and environmental impact. Further research is needed to understand the mechanisms through which nano-scale surface topography affects physicochemical interactions between foulant particles and a substrate surface.

5. Colloidal Adhesion on Micro-Patterned Surfaces[1]

Jianwei Ma[1], Jiangnan Zhang[2], Jun Lou[2], and Qilin Li[1]
1. Dept. of Civil and Environmental engineering, Rice University, Houston, Texas 77005
2. Dept. of Mechanical Engineering and Materials Science, Rice University, Houston, Texas 77005

5.1 Abstract

The effect of substratum topography on colloidal adhesion was investigated using silicon wafers with well-defined surface morphologies. Microscopic surface patterns consisting of orthogonal arrays of cuboid pillars or pits with different sizes and spacing between the features were fabricated by conventional photolithography and reactive ion etching. Adhesion of carboxyl modified polystyrene or poly (styrene-co-acrylic-acid) particles of 6 μm in diameter under favorable deposition conditions was markedly lower on all micro-patterned surfaces compared with that on the smooth control surface, even though the average adhesion force measured by atomic force microscopy was higher on patterned surfaces. Adhesion experiments using pillared patterns with systematically varied pillar size and spacing show that adhesion was the lowest when both the pillar size and the spacing were smaller than the size of the colloidal particle. However, the spacing between pillars seemed to be the controlling factor. Particle adhesion on the patterned surfaces was minimal when

[1] Manuscript to be submitted to *Langmuir*.
2 Jianwei Ma's contribution to the paper includes: design of the systematic micro-patterned surfaces; characterization of micro-patterned surfaces; colloidal particle adhesion on patterned surfaces.

the spacing between pillars was below a critical value, which was similar to the particle diameter. Meanwhile, there displayed unique distribution of colloidal particles on the micro-patterned surface: almost all the colloidal particles adhered on the edge of the pillars (between the pillars) when the spacing of patterns was smaller than that of the particle and fixed. The characteristic adhesion distribution of the colloidal particles on the micro-patterned surfaces was validated by the AFM adhesion force test. The results show colloidal adhesion depended on the relation between the colloidal size and characteristic dimensions of the micro-structures, which gives clue for future bio-adhesion control practice.

5.2 Introduction

Adhesion of colloidal particles or bacteria onto surfaces is a complex process affected by a variety of factors, among which surface morphology or topography is less understood. Previously, based on the laboratory and field observations, people concluded that adhesion of organisms, such as microorganisms[185], algal spores[186] and invertebrate larvae[187] is greater on rough surfaces than on smooth surfaces. Surface roughness was believed to affect the physical retention of colloidal particles or cells by enhancing surface contact, protection from hydrodynamic forces and desiccation[188]. Surface roughness could also arouse biological response by spatio-temporal positioning through site-specific gene expression, which would thus affect the interaction between cells and extracellular matrices, leading to different adhesion behavior of the organisms[96]. However, for most of the cases in previous

studies, the surface topography and physico-chemical properties of the test surfaces were not so well defined or undefined and sometimes the results are contradictory and misleading. It is necessary to use well defined surface topography to study the adhesion behavior to get safe and convincing conclusions.

Topographic surface structures that enhance and reduce microorganism adhesion relative to smooth surfaces have been reported. Bacterial adhesion was reported to increase as the surface roughness (R_a) caused by ordered arrays increased on electropolished steel[21]. On the contrary, bacterial adhesion decreased on microtopographic stainless steel surfaces that were generated by a one-directional polishing finish compared to the smooth surface[189]. A research done by Carman et al [27] showed that a biomimetically inspired surface topography (Sharklet AF^{TM}) containing 2 μm wide rectangular-like periodic features (4, 8, 12, 16 μm in length) spaced at 2 μm reduced *Ulva* spore settlement by 86%. More recently, studies on defined topographic surfaces showed that microbial adhesion on these surfaces was dependent on the dimensions of the surface feature relative to the microbial cell size[190].

The purpose of our study was to investigate how material surface topography affects physicochemical interactions between a particle and the substrate. Adhesion of micrometer sized particles on silicon surfaces with micro-patterns containing orthogonal arrays of cuboid pillars or pits was characterized. It was shown that all micro-patterns reduced particle adhesion compared to the smooth control surface. There existed a critical dimension under which the particle adhesion was minimal.

The reduction in particle adhesion was the greatest on patterns with the pillar size smaller than or similar to the size of the particle. Meanwhile, the particles exhibited unique distribution on the micro-patterned surface. Almost all the particles adhered on the edge of the pillars (between the pillars) when the spacing between the micro-pillars was smaller than that the diameter of the particles; while particles selectively adhered in the valley close to the pillar when the spacing between the micro-pillars was larger than the particle size..

5.3 Experimental Section

Materials

Silicon wafers (500 ± 25 μm thickness; 100 mm diameter, (111) orientation) polished on one side were obtained from Addison Engineering, Inc. (San Jose, CA).

Carboxylate modified latex (IDC, Eugene, OR, 4% solids) particles with a diameter of 6 μm and carboxyl modified poly (styrene-co-acrylic acid) (PSAA) green fluorescence microspheres of 6 μm in diameter (1.0% solids, Phosphorex, Inc) were used as model colloidal particles. Over 99 wt% of the fluorescent microsphere solid is PSAA with styrene being the predominant unit, and there is approximately 1 wt% fluorescent dye in the polymer microspheres. The excitation wavelength for the particle is 480 nm and the emission wavelength is 509 nm. The density of the carboxyl function groups on PSAA is 6.02×10^7/sphere.

All chemical reagents used were reagent or ACS Grade. Reagent-grade 190 proof ethanol (95%) was obtained from DECON Labs, Inc (King of Prussia, PA). All

solutions and suspensions were prepared using ultrapure water ($\geqslant$18.1 mega Ω-cm) generated by an E-Pure system (Barnstead, VWR, Batavia, IL).

Micro-patterned surface fabrication

For most experiments, the wafers were cut into smaller chips of 0.8 cm × 1.2 cm in size using a diamond-tipped scribe. The wafer samples were cleaned with Piranha solution at 110 to 130 °C for 60 minutes to remove organic contaminants. The samples were then dried with ultrapure N_2 and used for pattern fabrication. Using standard photolithography methods, arrays of 1 mm × 1 mm patterns consisting of microscopic features of different dimensions were manufactured on a single silicon chip with a 0.3 mm distance between patterns. Briefly, the clean silicon chips were first baked at 150 °C for 10 to 15 minutes. Two drops of S1813 photoresist were then spin-coated on the chips at 5000 RPM. After deploying a Mask Aligner (Suss Mask Aligner MJB4) to expose the chips (mask from Fineline Imaging, Colorado Springs, CO), develop 319 was subsequently used to remove the residual photoresist. The residual water on the chips was blown dry. A chrome film of several micrometers in thickness was sputtered on the chips (CRC-150 Sputter Coater). The chrome coated chips were then boiled in Remover 1165 at 100 °C for 60 minutes. A standard Reactive Ion Etch (Minilock-Phantom III Trion RIE) procedure was employed to etch chip to obtain 2 to 3 microns in feature height. Also, the smooth control surface tested was etched under the same conditions as the patterns in order to ensure identical surface chemistry.

The patterns fabricated consisted of orthogonal arrays of cuboidal pillars or pits. The first batch of patterns was designed to include a wide range of feature (i.e., pillar

or pit) size and spacing between features. The two series of patterns were fabricated to independently investigate the effect of feature size and spacing: one series consisted of cuboidal pillars of 5 μm to 40 μm in size with a fixed spacing of 5 μm in all the patterns; the other series consisted of cuboidal pillars of identical sizes of 5 μm with the spacing between pillars varying from 5 μm to 40 μm (characterized by SEM, XPS, Profilometry).

Colloidal Particle Adhesion Experiments

Before each experiment, the micro-patterned as well as the control silicon chips were cleaned using the following protocol. The samples were first soaked in 2% Extran MA02 solution for 2 hours, followed by rinsing with ethanol and ultrapure water for 5 times. Then, they were sonicated at room temperature in a 2% RBS 35 detergent solution for 20 min and rinsed again with ethanol and ultrapure water. The samples were subsequently soaked in the NOCHROMIX solution (GODAX Laboratories, Inc., Cabin John, MD) for 24 h and thoroughly rinsed with ultrapure water, after which particulate free ultrapure N_2 was used to dry the surfaces.

The clean patterned and control surfaces were placed side by side in the same well of a six-well incubator plate, cleaned with detergent and dried with particle-free nitrogen. Then 5 ml of the background electrolyte solution (100 mM NaCl with pH adjusted to 4 using HCl solution) was added into the well. The stock suspension of PSAA particles (8.4×10^7/ml) was first sonicated for 15 min to ensure good dispersion, 37.5 μl of which was then added into the test well to achieve a particle concentration of 2×10^6/ml. The incubator plate was then wrapped in aluminum foil,

put on an orbital shaker table (VWR OS-500, West Chester, PA) and incubated at room temperature for 30 min at 50 rpm. After incubation, the samples were gently rinsed to remove unattached or loosely attached particles. In order to avoid exposure to the air-water-solid interface, which causes strong surface forces potentially disturbing the adhered particles, a rinsing protocol was developed without taking the samples out of solution. In each rinse, the residual particle suspension or cleaning solution was pipette out but leaving enough to keep the test samples submerged. The cleaning solution, i.e., the background solution used in the adhesion experiments, was then added to the container and the container was gently hand shaken horizontally in a circular motion for 2 min. This step was repeated 5 times. After the last rinse, a glass slip cover was put on the submerged test samples, and the samples were taken out for analysis.

All the apparatuses were extremely carefully cleaned to avoid any possible particle contamination. Experiments were repeated at least three times.

After rinsing, the samples were imaged with an upright with an Axioplan 2 epifluorescence microscope (Carl Zeiss, Oberkochen, Germany). Images were acquired with a CoolSnap HQ camera (Photometrics, Tucson, Ariz.) controlled by Metamorph 7 imaging software (Molecular Devices Corporation, Sunnyvale, CA). Five images were acquired on each pattern and the images were analyzed using the ImageJ software [174] to obtain the average particle number on each pattern.

AFM Adhesion Force Measurement

Adhesion force between the PSAA particle and the different pattern surfaces

were measured using atomic force microscopy (AFM). The measurements were performed using a colloidal probe prepared by attaching a PSAA particle (the same as those used in the adhesion experiments) to the end of a silicon AFM probe (PPP-NCH-W, NanoSensors, Neuchatel, Switzerland) with spring constant 0.44 N/m with a 24 hour epoxy (Hardman, Wilmington, CA) using a micromanipulator (DC-3KS Rechts, Marzhauser, Germany). The colloid probe was examined under an optical microscope after 24 hours of curing and stored in dard at 4 °C until use. Before use, the colloid probe was examined again by scanning an AFM calibration surface consisting of sharp arrays of spikes using the colloid probe. No contamination of epoxy was found on the surface of the PSAA particle probe (Figure 5.1).

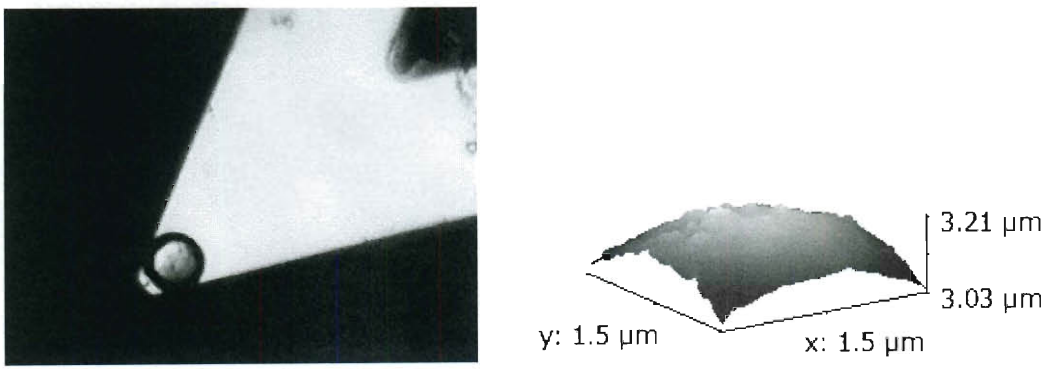

(a) (b)

Figure 5. 1. (a) Microscopic image of the CML colloid probe and (b) AFM image of the colloid probe tip

All AFM experiments were performed in a liquid cell filled with the same background solution used in the adhesion, i.e., 100 mM NaCl with pH adjusted to 4. In order to quantify the adhesion forces between silicon pattern and the AFM probe, force vs.

distance spectroscopy was run on different dimension arrays and the amount of adhesion was measured Scan was done over an area of 40μm×40μm. The cantilever tip was first located on top of the pillar; then the scan was done line by line. To convert voltage signals into units of force, the following equation was used $F_f = \kappa \cdot V$, in which κ is the calibration factor. A robust procedure has also been developed in this study to construct an adhesion force map consisting of 1024 force-distance spectroscopy curves in each scan to characterize adhesion characteristics of the samples with proper statistical treatments.

5.4 Results and Discussion

5.4.1 Characterization of the Micro-patterned Surface

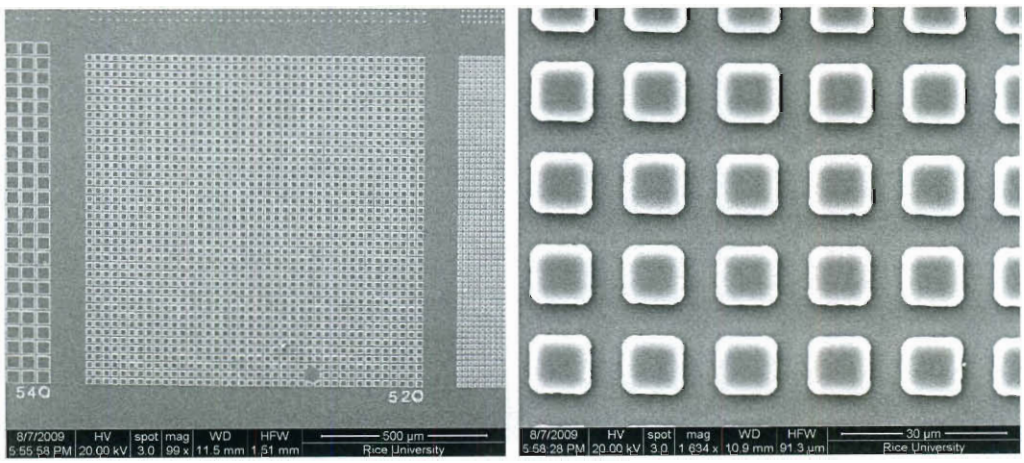

Figure 5. 2. Representative SEM image of the micro-patterned surface (s: 5μm, d: 12μm)

The photolithography-RIE method used was able to produce precise and reproducible micro-patterns. Figure 5.2 shows an example of the patterns fabricated.

The actual pillar size (11.89 μm) and spacing (5.05 μm) matched well with the design (12 μm and 5 μm for pillar size ad spacing, respectively)

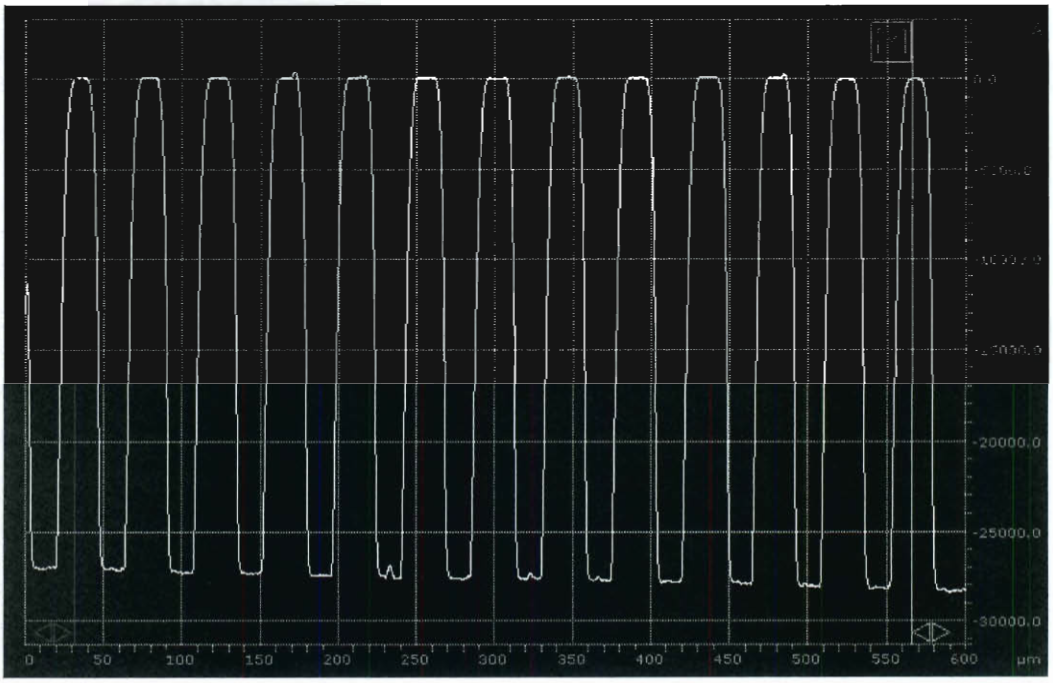

Figure 5. 3. Representative profile of the micro-pillared structure obtained by a Veeco Daktek profilometer showing the perfect uniformity

The height of the microscale surface features was measured by profilometry (Veeco DekTak 6M stylus profilometer, Plainview, NY). Vertical profile of the patterns (see Figure 5.3 for an example) showed the reproducibility of the micro-sized structures across the whole pattern surface. The pillars/pits were about 2.5-3 μm in height/depth.

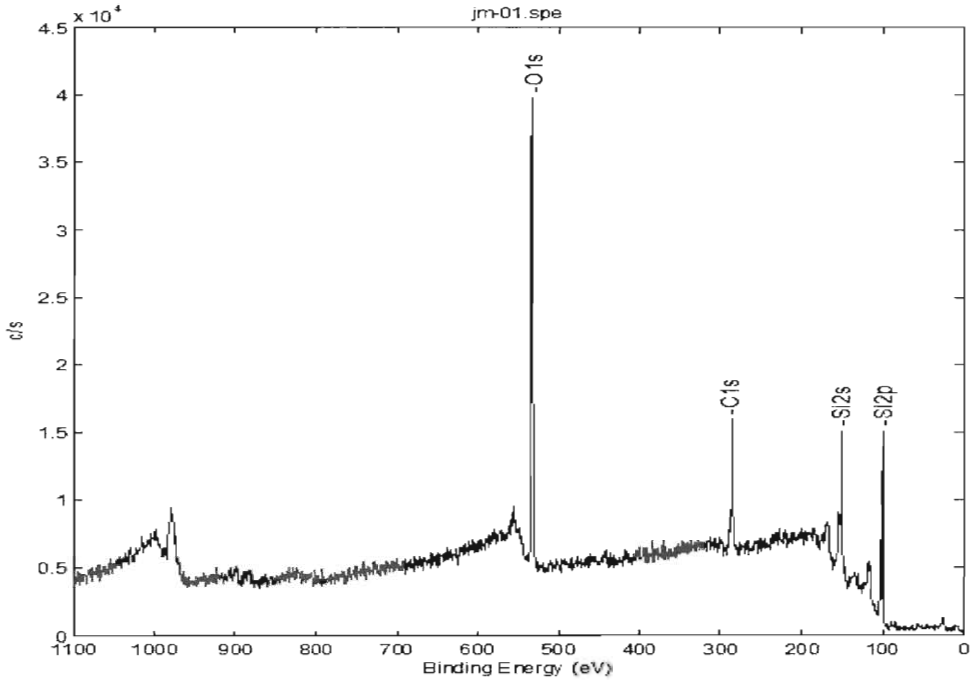

Figure 5. 4. XPS Surface Chemical Element Analysis for the Micro-patterned Surface

Because surface chemistry plays an important role in particle adhesion, it is important to ensure that all test surfaces have the same surface chemistry so that the observed difference in adhesion behavior can be exclusively attributed to surface morphology. Because chromium was used as a protecting material in photolithography, there was concern that chromium residual might be present in areas not exposed to RIE leading to chemical heterogeneity on the micro-patterned surfaces. Therefore, XPS analysis was performed to determine surface chemical composition. Figure 5.4 shows a typical XPS survey spectrum acquired from the micro-patterned surface. Chemical elements detected included Si, C and O, and the surfaces consisted primarily of SiO_2. No chromium or other contaminants were detected on any sample surfaces. Based on these results, the micro-patterning process did not cause detectable changes in surface chemical composition.

5.4.2 PSAA Particle Adhesion on Patterned Surfaces

The first batch of samples included patterns with a wide range of feature size and spacing. Results of the particle adhesion experiments are summarized in Table 5.1. From the table, we can see that patterns with small spacing (D12.47S6.24, D10.30S3.92 for pillars; D12.47S8.31, D22.87S8.31) can significantly reduce the adhesion of particles on the surface.

Table 5. 1. Particle adhesion on patterned surface with different dimensions for both pillars and pits

Pillar	**Different Surfaces**		**NO.1**	**NO.2**	**NO.3**	**Average**	**95% Confidence lower limit**	**95% Confidence upper limit**	**Error**
	D	**S**							
*	–	–	177	188	173	179	160.04	198.63	19.30
	27.72	18.03	91	93	94	93	88.87	96.46	3.79
	12.47	6.24	6	6	2	5	-1.07	10.40	5.74
	31.18	25.64	32	41	42	38	24.65	52.01	13.68
	36.04	44.35	27	29	47	34	6.97	61.70	27.36
	15.24	24.26	102	79	99	93	62.27	124.39	31.06
	16.64	33.95	66	60	47	58	33.54	81.79	24.13
	21.48	18.03	114	152	153	140	84.44	194.90	55.23
	10.30	3.92	6	7	5	6	3.52	8.48	2.48
	13.16	15.24	114	90	89	98	62.51	132.83	35.16
	35.34	65.86	125	95	97	106	64.00	147.33	41.67
	27.02	81.76	87	52	53	64	14.50	113.50	49.50
	18.71	38.11	57	66	53	59	42.13	75.21	16.54
	18.71	50.59	57	50	64	57	39.61	74.39	17.39
	18.03	58.91	84	62	89	78	42.65	114.02	35.68
	17.32	13.86	40	51	54	48	30.02	66.64	18.31
	29.10	49.20	38	37	25	33	15.36	51.30	17.97
	31.18	63.05	29	46	33	36	13.92	58.08	22.08
	14.55	33.95	51	43	37	44	26.22	61.11	17.45
Pit									
	31.87	10.39	78	78	124	93	27.36	159.31	65.97

	12.47	8.31	5	10	3	6	-2.96	14.96	8.96
	32.56	29.1	64	42	56	54	26.34	81.66	27.66
	22.87	8.31	8	8	5	7	2.70	11.30	4.30
	21.48	16.63	73	54	50	59	28.47	89.53	30.53
	33.26	45.73	39	41	20	33	4.54	62.13	28.79
	31.87	63.75	27	31	19	26	10.49	40.84	15.18
	22.87	24.94	35	35	46	39	22.89	54.44	15.78
	23.56	30.49	41	55	42	46	26.60	65.40	19.40

D: pillar/pit size (unit: μm)
S: spacing between pillars and pits (unit: μm)
*: flat surface

For better comparison, particle adhesion on all test surfaces was plotted as a function of surface feature size and spacing (Figure 5.5). As shown in Figure 5.5, all patterned surfaces exhibited lower particle adhesion than the smooth control surface. More importantly, particle adhesion in general decreased with decreasing feature size and spacing. Among all the surfaces tested those with spacing similar to or smaller than the particle size (6 μm) had minimal particle adhesion. For example, D12.47S6.24 and D10.30S3.92 for pillar pattern significantly reduced particle adhesion.

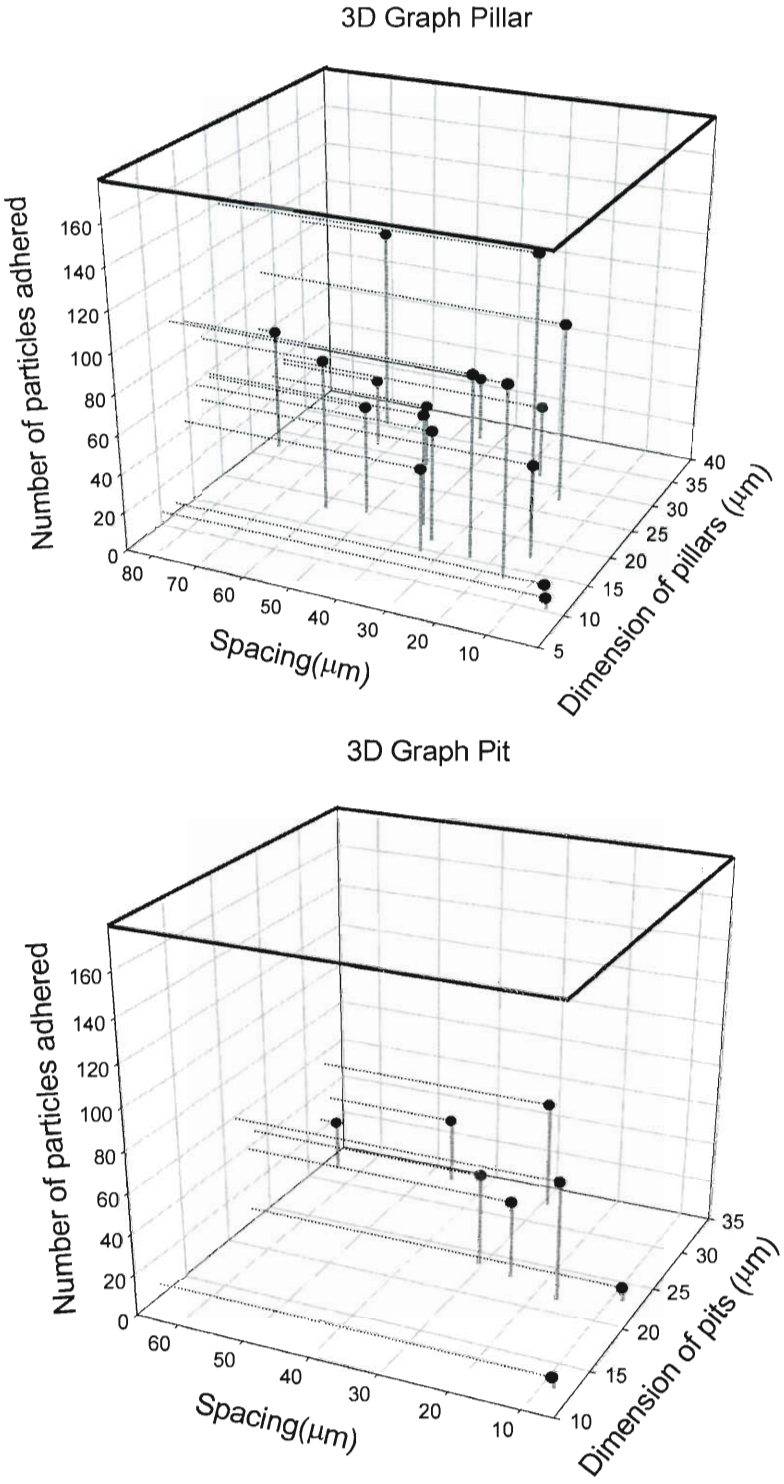

Figure 5. 5. 3-D plot of particle adhesion on patterned surface. (The top surface indicates the particle adhesion on the smooth surface). CML particles were used in these experiments.

Distribution of the adhered particles strongly depended on the surface patterns. Although particles were randomly distributed on the control surfaces, their distribution appeared to be guided by surface features on the patterned surfaces (Figure 5.6). On pillar patterns with spacing significantly larger than the particle size, almost all particles adhered to the side of the pillars with very few (if any) on the top of the pillars; on pillar patterns with spacing similar to or smaller than the particle size, particles randomly distributed over the valleys. Almost all the particles adhered on the edges within the pits for the pit patterns.

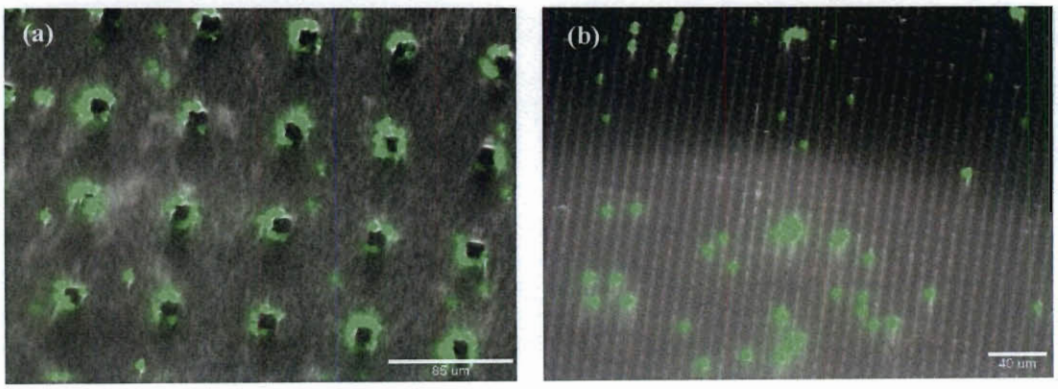

Figure 5. 6. PSAA particle adhesion on different patterns (a) D11.76S54.66; (b) D8.36S3.61

In order to independently investigate the effect of feature size and spacing on particle adhesion, experiments were performed using two series of pillar patterns with systematically varied pillar size and spacing (Table 5.2). Results are summarized in Figure 5.7. Again, all patterned surfaces exhibited markedly lower particle adhesion than the smooth control surface.

Table 5. 2. Dimensions of the two series of pillar patterns with systematically varied pillar size and spacing

Height (μm)	Spacing (μm)	Diameter (μm)
2~3	5	5
2~3	5	6
2~3	5	7
2~3	5	11
2~3	5	12
2~3	5	20
2~3	5	40

Height (μm)	Diameter (μm)	Spacing (μm
2~3	5	5
2~3	5	6
2~3	5	7
2~3	5	11
2~3	5	12
2~3	5	20
2~3	5	40

When the spacing between pillars was fixed at 5 μm, particle adhesion was very low, 1.67% to 4.14% of that on the control surface, for small pillars (≤ 7 μm). However, the number of particles adhered increased dramatically as the size of the pillars increased beyond 7 μm. This is consistent with observations in a previous study[191]. It was explained that when the scale of the micro-structure is much larger than the size of the colloidal particle, micro-roughness is relatively unimportant, i.e., the particles see a smooth surface. However, in most cases, particles preferentially adhered over the gaps between the pillars (edge effect particles which adhere to the side of pillar or between two pillars), even though there was much surface area available on the pillar top (Figure 5.7(b), Figure 5.8).

Interestingly, when the pillar was fixed at 5 μm, very few particles adhered to the

surface even when the spacing of the pillars was much larger than the size of the particles; among the few adhered, particles preferably adhered in the valley within close proximity to the pillars (Figure 5.7 (d), Figure 5.8). These results suggest that the pillar size plays a key role in particle adhesion on a micro-patterned surface; particle adhesion is minimized when the pillar size is smaller than the size of the particle.

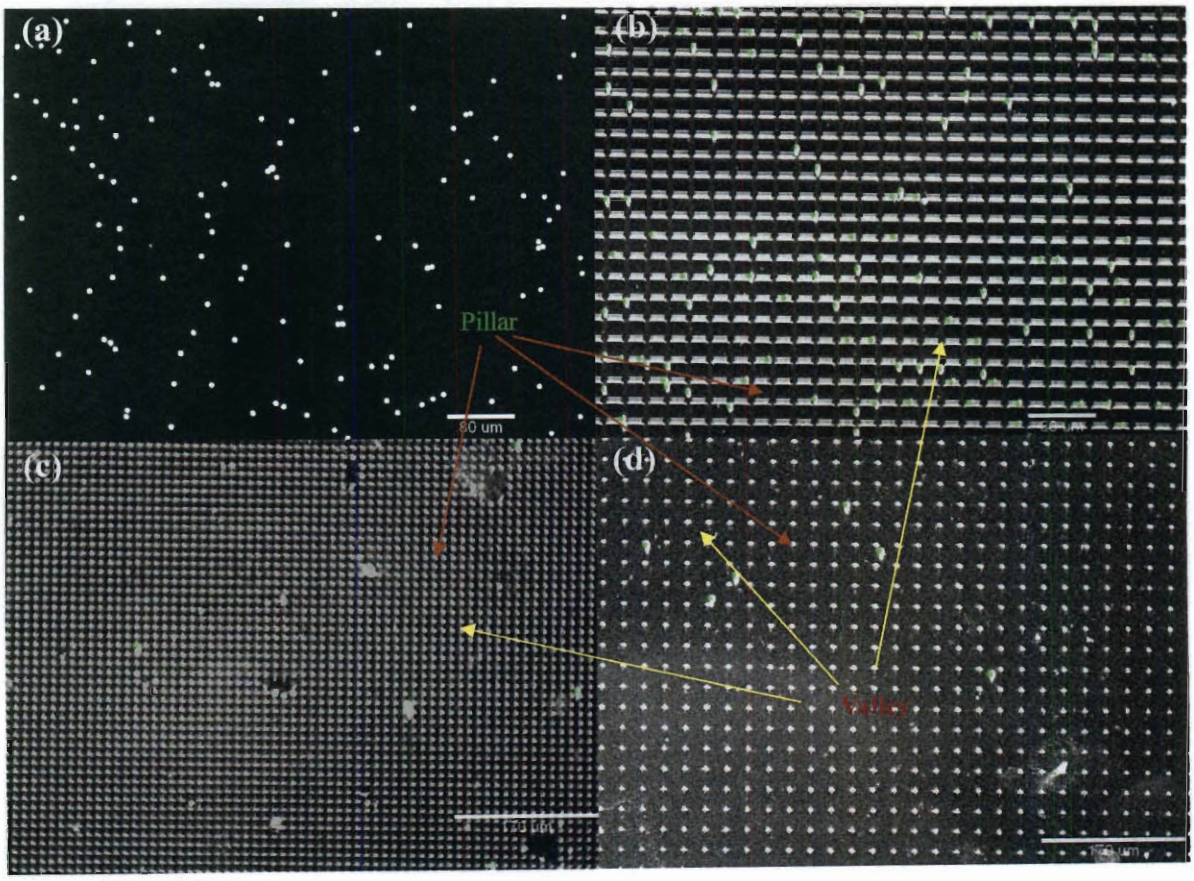

Figure 5. 7. Carboxyl Modified Fluorescence Microsphere Particle Distribution on (a) Flat surface; (b) Micro-Patterned Surface (s 5 μm, d 20μm) (scale bar: 80μm); (c) Micro-Patterned Surface (s 5 μm, d 6μm); (d) Micro-Patterned Surface (d 5 μm, s 20μm) (scale bar: 80μm)

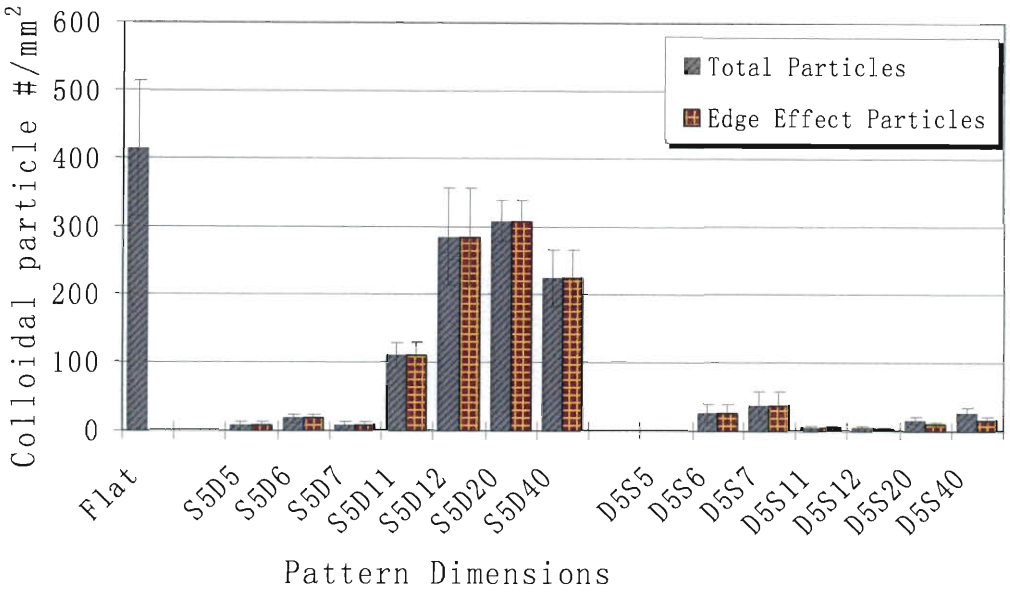

Figure 5. 8. Number of colloidal particles attached to different micro-patterned surfaces. PSAA particles were used in these experiments.

5.4.3 Adhesion forces on the patterned surfaces

The adhesion force between a PSAA particle and a patterned sample surface was determined by AFM in the same background solution used in the adhesion experiments. Figure 5.9 shows the adhesion force maps over a 40 μm × 40 μm area on two patterned surfaces. The scanning area was chosen to include both pillars and valleys so that the average adhesion force can represent that over the whole pattern. With a large pillar size and fixed spacing of 5 μm, the adhesion force was the highest on the edge of the pillars. This is consistent with the preferable adhesion on pillar edges observed in the particle adhesion experiments (Figure 5.7 (b)). On the contrary, when the pillar size is small compared to the spacing, the adhesion force is much lower on the pillars than the rest of the surface, consistent with the observation that

particles only adhered in the valley (Figure 5.7 (d)). Within the valleys, particles adhered close to the pillars presumably because they can gain hydrodynamic shelter near the pillar walls. Adhesion forces on different surfaces are shown in table 5.3.

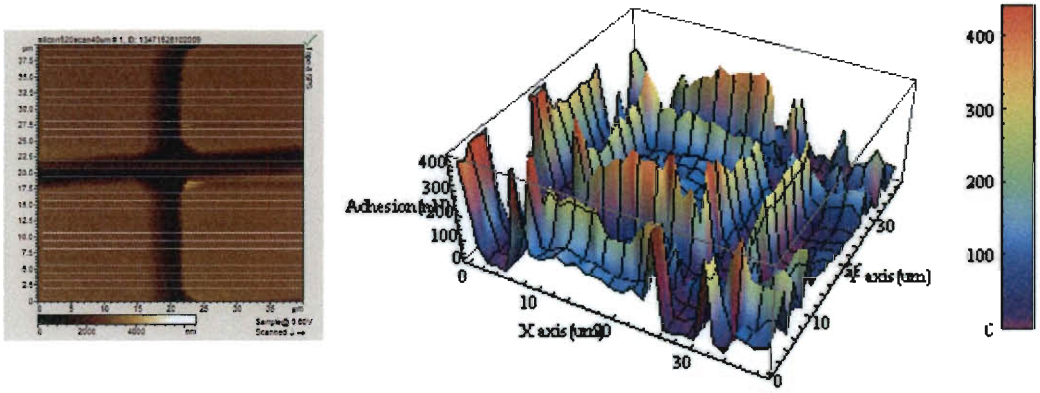

(a)

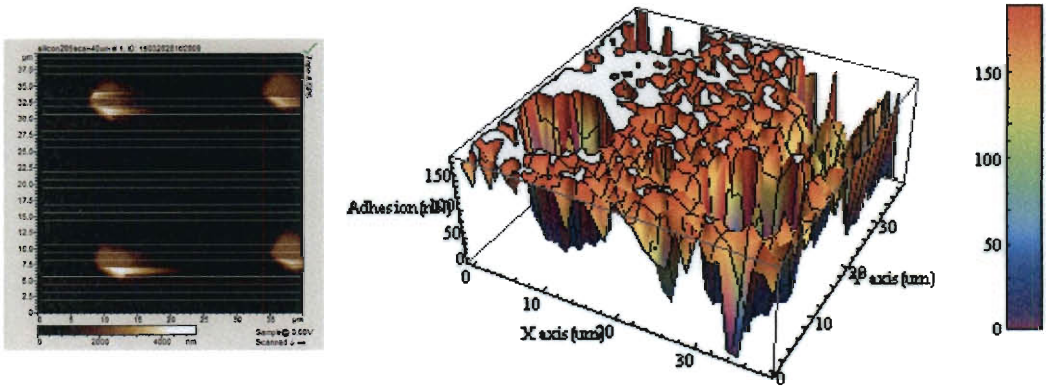

(b)

Figure 5. 9. Adhesion force distribution from colloidal-tipped AFM test (a) spacing 5 μm, pillar size 20 μm; (b) spacing 20 μm, pillar size 5 μm. Scan area 40 μm × 40 μm.

Table 5. 3. Adhesion force on different surfaces by AFM

Different Surfaces	Scan Area(μm×μm)	Mean Adhesion Force(nN)
S5D7	40 μm×40 μm	103.087
S12D5	40 μm×40 μm	232.834
S20D5	40 μm×40 μm	137.986
D5D12	40 μm×40 μm	105.954
S5D20	40 μm×40 μm	101.820
Flat Surface	40 μm×40 μm	72.329

5.5 Conclusion

Although surface topography is known to play an important role in particle adhesion, its actual effect was unclear. Using engineered surfaces with well-defined microscopic surface patterns, we demonstrated that adhesion of micro-sized particles was strongly influenced by the size and spacing of micro-scale surface features. Compared to the smooth control surface, all micro-patterns significantly reduced particle adhesion. In general, particle adhesion decreased with decreasing surface feature size and spacing. There seemed to be a critical surface feature dimension below which particle adhesion was minimized; the critical dimension was similar to the particle size. The micro-patterns were found to strongly modulate the surface adhesion force, which in turn governed distribution of particles o the surface.

However, the changes in adhesion force were not able to explain the overall reduced particle adhesion on the micro-patterned surfaces (Table 5.3). Changes in hydrodynamics were hypothesized to play an important role as well. Our work suggests that surface-patterning could be a potential approach to particle fouling control. More complete understanding of the mechanisms through which surface topography affects particle adhesion is necessary in order to design patterned surfaces to prevent particle or bacterial adhesion.

6. Conclusions and Future Research

6.1 Conclusions

More and more endeavor has been made towards imitating nature's smartness to make bio-inspired engineered materials or devices, among which self-cleaning (or anti-fouling) exhibited by many plants such as lotus leaf, taro leaf, etc has been raised great attention in recent years. It is believed that surface topography plays significant role in making this kind of unique property possible. In order to adopt this self-cleaning property in membrane water filtration systems in which membranes are submerged in solution, it is of great importance to investigate the particle adhesion property on these nature self-cleaning surface under submerged condition and get some hint from it. We show in this study that more particle and bacterial adhesion took place on the edge of the micro-structure units or between them throughout the taro leaf surface where there were sparse nano-structures than the valley and center of micro-structure units where there were dense nano-structures, indicating that nano-structure which is much smaller than the dimension of particle and bacterium plays the role of reducing the particle and bacterial adhesion.

Inspired by the results from adhesion on nature self-cleaning surface under, well defined engineered micro-patterned surface with orthogonal arrays of cuboid pillars were fabricated by RIE and photolithography with different dimensions (varied pillar size and spacing between pillars), the lower limit dimension of which was a bit smaller than the size of the particle tested. Our study showed that the number of

particles adhered on the micro-patterned surface was smaller than on the smooth controls, especially when the dimension (spacing) of patterns is close to/smaller than the size of the colloid. Meanwhile, there displayed unique distribution of colloidal particles on the micro-patterned surface: almost all the colloidal particles adhered on the edge of the pillars (between the pillars) when the spacing of patterns was a bit smaller than that of the particle and fixed, while there was dramatically reduced number of particles on patterns with fixed size of pillars and specified variations of spacing.

6.2 Future Research

More experiments can be performed on this topic in order to reveal the impact of surface topography on particle/bacterial adhesion. Potential future research work can include the following parts:

(1) Particle/bacterial adhesion on patterned surface under continuous flow condition

It is very important to know the adhesion property under flow condition as in many cases (e.g. membrane water filtration process, blood vessels, ship hulls etc) there are dynamic flow accompanying the adhesion. Also, in the stagnant adhesion experiment, the "slight-rinsing" process will affect the adhering bacteria, which happened for all the cases. Though the original goal for the rinsing is to remove the loosely adhering bacteria, yet it raises couple of concerns as to the magnitude of the rinsing forces applied, the definition of "loosely adhering" bacteria and percentage of total adhering population removed by rinsing. To resolve both, a parallel plate flow

chamber under controlled hydrodynamic conditions can be adopted.

(2) Bacterial adhesion on nano-patterned surface

The nanoscale topography of artificial materials is known to play a significant role in interactions between cells and surfaces; meanwhile, our study gave the hint that nano-topographic structures affect bacterial adhesion and distribution on nature self-cleaning surface. A detailed understanding and ultimate manipulation of these interactions is of extreme importance in many different areas. Although cellular responses to nanoscale surface features have been widely reported to be altered compared to the situation for planar control surfaces, the underlying mechanisms of cell sensing, intercellular signaling and long-term response to surface nanotopography are still very challenging and timely areas of research need to be addressed.

(3) Patterned surface adhesion model development

Theoretical calculation based on DLVO (XDLVO) incorporating hydrodynamic effect should be addressed on particle adhesion on patterned surface to better elucidate the topography effect and validate the experimental results.

References

1. Mineur, F., et al., *Hull fouling on commercial ships as a vector of macroalgal introduction.* Marine Biology, 2007. **151**(4): p. 1299-1307.
2. Herzberg, M. and M. Elimelech, *Biofouling of reverse osmosis membranes: Role of biofilm-enhanced osmotic pressure.* Journal of Membrane Science, 2007. **295**(1-2): p. 11-20.
3. Baker, J.S. and L.Y. Dudley, *Biofouling in membrane systems - A review.* Desalination, 1998. **118**(1-3): p. 81-89.
4. Knoell, T., et al., *Biofouling potentials of microporous polysulfone membranes containing a sulfonated polyether-ethersulfone/polyethersulfone block copolymer: correlation of membrane surface properties with bacterial attachment.* Journal of Membrane Science, 1999. **157**(1): p. 117-138.
5. Costerton, J.W., P.S. Stewart, and E.P. Greenberg, *Bacterial biofilms: A common cause of persistent infections.* Science, 1999. **284**(5418): p. 1318-1322.
6. Flemming, H.C., Schaule G, *Measures against biofouling.* Microbially influenced corrosion of materials- scientific and technological aspects, ed. S.W. Heitz E, Flemming H-C. 1996, Berlin Heidelberg New york: Springer. 121-139.
7. Flemming, H.C., *Biofouling in water systems - cases, causes and countermeasures.* Applied Microbiology and Biotechnology, 2002. **59**(6): p. 629-640.
8. LeChevallier, M., *biocides and the current status of biofouing control in water systems.* Biofouling and biocorrosion in industrial water systems, ed. H.C. Flemming, Geesey GG. 1991, Berlin Heidelberg New york: Springer. pp113-132.
9. Okabe, S.e.a., *Anaerobic SRB biofilms in industrial water systems: a process analysis.*, in *Biofouling and Biocorrosion in industrial water systems*, G.G. Geesey, Editor. 1994, Lewis Publishers: Boca Raton. p. 189-204.
10. An, Y.H., Friedman, R.J., *Handbook of Bacterial Adhesion.* 2000, Totowa, New Jersey: Human Press Inc.
11. Schmidt, D.L., et al., *Contact angle hysteresis, adhesion, and marine biofouling.* Langmuir, 2004. **20**(7): p. 2830-2836.
12. Zhao, Q., et al., *Effect of surface free energy on the adhesion of biofouling and crystalline fouling.* Chemical Engineering Science, 2005. **60**(17): p. 4858-4865.
13. Mrksich, M., *A surface chemistry approach to studying cell adhesion.* Chemical Society Reviews, 2000. **29**(4): p. 267-273.
14. Callow, M.E. and R.L. Fletcher, *The Influence of Low Surface-Energy Materials on Bioadhesion - a Review.* International Biodeterioration & Biodegradation, 1994. **34**(3-4): p. 333-348.
15. Kantlehner, M., et al., *Surface coating with cyclic RGD peptides stimulates*

osteoblast adhesion and proliferation as well as bone formation. Chembiochem, 2000. **1**(2): p. 107-114.

16. Li, X.Q., T.Q. Liu, and Y.T. Chen, *The effects of the nanotopography of biomaterial surfaces on pseudomonas fluorescens cell adhesion.* Biochemical Engineering Journal, 2004. **22**(1): p. 11-17.
17. Boyd, R.D., et al., *Use of the atomic force microscope to determine the effect of substratum surface topography on bacterial adhesion.* Langmuir, 2002. **18**(6): p. 2343-2346.
18. Shellenberger, K. and B.E. Logan, *Effect of molecular scale roughness of glass beads on colloidal and bacterial deposition.* Environmental Science & Technology, 2002. **36**(2): p. 184-189.
19. Scheuerman, T.R., A.K. Camper, and M.A. Hamilton, *Effects of substratum topography on bacterial adhesion.* Journal of Colloid and Interface Science, 1998. **208**(1): p. 23-33.
20. Taylor, R.L., et al., *The influence of substratum topography on bacterial adhesion to polymethyl methacrylate.* Journal of Materials Science-Materials in Medicine, 1998. **9**(1): p. 17-22.
21. Medilanski, E., et al., *Influence of the surface topography of stainless steel on bacterial adhesion.* Biofouling, 2002. **18**(3): p. 193-203.
22. Teughels, W., et al., *Effect of material characteristics and/or surface topography on biofilm development.* Clinical Oral Implants Research, 2006. **17**: p. 68-81.
23. Hilbert, L.R., et al., *Influence of surface roughness of stainless steel on microbial adhesion and corrosion resistance.* International Biodeterioration & Biodegradation, 2003. **52**(3): p. 175-185.
24. BoulangePetermann, L., J. Rault, and M.N. BellonFontaine, *Adhesion of Streptococcus thermophilus to stainless steel with different surface topography and roughness.* Biofouling, 1997. **11**(3): p. 201-&.
25. Beck, U., et al., *Purification of real surfaces.* Chemie Ingenieur Technik, 2005. **77**(12): p. 1942-1946.
26. Flint, S.H., J.D. Brooks, and P.J. Bremer, *Properties of the stainless steel substrate, influencing the adhesion of thermo-resistant streptococci.* Journal of Food Engineering, 2000. **43**(4): p. 235-242.
27. Carman, M.L., et al., *Engineered antifouling microtopographies - correlating wettability with cell attachment.* Biofouling, 2006. **22**(1): p. 11-21.
28. Hoipkemeier-Wilson, L., et al., *Antifouling potential of lubricious, micro-engineered, PDMS elastomers against zoospores of the green fouling alga Ulva (Enteromorpha).* Biofouling, 2004. **20**(1): p. 53-63.
29. Schumacher, J.F., et al., *Species-specific engineered antifouling topographies: correlations between the settlement of algal zoospores and barnacle cyprids.* Biofouling, 2007. **23**(5): p. 307-317.
30. Schumacher, J.F., et al., *Engineered antifouling microtopographies - effect of feature size, geometry, and roughness on settlement of zoospores of the green alga Ulva.* Biofouling, 2007. **23**(1): p. 55-62.

31. Schumacher, J.F., et al., *Engineered nanoforce gradients for inhibition of settlement (attachment) of swimming algal spores.* Langmuir, 2008. **24**(9): p. 4931-4937.
32. Curtis, A.S.G., et al., *Cells react to nanoscale order and symmetry in their surroundings.* Ieee Transactions on Nanobioscience, 2004. **3**(1): p. 61-65.
33. Curtis, A.S.G., et al., *Substratum nanotopography and the adhesion of biological cells. Are symmetry or regularity of nanotopography important?* Biophysical Chemistry, 2001. **94**(3): p. 275-283.
34. Turner, S., et al., *Cell attachment on silicon nanostructures.* Journal of Vacuum Science & Technology B, 1997. **15**(6): p. 2848-2854.
35. Clark, P., S. Britland, and P. Connolly, *Growth Cone Guidance and Neuron Morphology on Micropatterned Laminin Surfaces.* Journal of Cell Science, 1993. **105**: p. 203-212.
36. Fujimoto, K., et al., *Cell activation by the micropatterned surface with settling particles.* Journal of Biomaterials Science-Polymer Edition, 1997. **8**(11): p. 879-891.
37. Van de ven, T.G.M., *Colloidal hydrodynamics*. Colloidal science;4. Vol. xvi. 1989, London;San Diego: Academic Press. 582.
38. Busscher, H.J. and H.C. van der Mei, *Physico-chemical interactions in initial microbial adhesion and relevance for biofilm formation.* Adv Dent Res, 1997. **11**(1): p. 24-32.
39. McEldowney, S. and M. Fletcher, *Variability of the Influence of Physicochemical Factors Affecting Bacterial Adhesion to Polystyrene Substrata.* Applied and Environmental Microbiology, 1986. **52**(3): p. 460-465.
40. Curtis, A.S.G., et al., *Adhesion of Cells to Polystyrene Surfaces.* Journal of Cell Biology, 1983. **97**(5): p. 1500-1506.
41. Tsuneda, S., et al., *Extracellular polymeric substances responsible for bacterial adhesion onto solid surface.* Fems Microbiology Letters, 2003. **223**(2): p. 287-292.
42. Abbott, A., P.R. Rutter, and R.C.W. Berkeley, *The Influence of Ionic-Strength, Ph and a Protein Layer on the Interaction between Streptococcus-Mutans and Glass Surfaces.* Journal of General Microbiology, 1983. **129**(FEB): p. 439-445.
43. Bos, R., H.C. vanderMei, and H.J. Busscher, *Influence of ionic strength and substratum hydrophobicity on the co-adhesion of oral microbial pairs.* Microbiology-Uk, 1996. **142**: p. 2355-2361.
44. Orstavik, D., *Sorption of Streptococcus-Faecium to Glass.* Acta Pathologica Et Microbiologica Scandinavica Section B-Microbiology, 1977. **85**(1): p. 38-46.
45. Harber, M.J., R. Mackenzie, and A.W. Asscher, *A Rapid Bioluminescence Method for Quantifying Bacterial Adhesion to Polystyrene.* Journal of General Microbiology, 1983. **129**(MAR): p. 621-632.
46. Deighton, M. and R. Borland, *Regulation of Slime Production in Staphylococcus-Epidermidis by Iron Limitation.* Infection and Immunity, 1993. **61**(10): p. 4473-4479.

47. Krajewska-Pietrasik, D., M. Wykrota, and Z. Sidorczyk, *The influence of growth temperature on Staphylococcus aureus adhesion to collagen.* Medycyna Doswiadczalna i Mikrobiologia, 1997. **49**(3-4): p. 123-130.
48. McEldowney, S., *Effect of Cadmium and Zinc on Attachment and Detachment Interactions of Pseudomonas-Fluorescens H2 with Glass.* Applied and Environmental Microbiology, 1994. **60**(8): p. 2759-2765.
49. Derjaguin, B. and L. Landau, *Theory of Stability of Highly Charged Liophobic Sols and Adhesion of Highly Charged Particles in Solutions of Electrolytes.* Zhurnal Eksperimentalnoi I Teoreticheskoi Fiziki, 1945. **15**(11): p. 663-682.
50. Overbeek, J.T., *Colloid Stability in Aqueous and Non-Aqueous Media - Introductory Paper.* Discussions of the Faraday Society, 1966(42): p. 7-&.
51. Verwey, E.J.W., *Theory of the Stability of Lyophobic Colloids.* Journal of Physical and Colloid Chemistry, 1947. **51**(3): p. 631-636.
52. Hermansson, M., *The DLVO theory in microbial adhesion.* Colloids and Surfaces B-Biointerfaces, 1999. **14**(1-4): p. 105-119.
53. Vanoss, C.J., *Acid-Base Interfacial Interactions in Aqueous-Media.* Colloids and Surfaces a-Physicochemical and Engineering Aspects, 1993. **78**: p. 1-49.
54. Skvarla, J., *The Role of Interfacial Interactions in the Particle/Bubble Attachment.* Journal of Dispersion Science and Technology, 1991. **12**(3-4): p. 349-380.
55. Vanoss, C. and R.J. Good, *Relation between the Apolar and Polar Components of the Interaction Energy between the Chains of Nonionic Surfactants and Their Cmc in Water.* Journal of Dispersion Science and Technology, 1991. **12**(1): p. 95-105.
56. Hoek, E.M.V. and G.K. Agarwal, *Extended DLVO interactions between spherical particles and rough surfaces.* Journal of Colloid and Interface Science, 2006. **298**(1): p. 50-58.
57. Brant, J.A. and A.E. Childress, *Membrane-colloid interactions: Comparison of extended DLVO predictions with AFM force measurements.* Environmental Engineering Science, 2002. **19**(6): p. 413-427.
58. Bhattacharjee, S., C.H. Ko, and M. Elimelech, *DLVO interaction between rough surfaces.* Langmuir, 1998. **14**(12): p. 3365-3375.
59. Bhattacharjee, S. and M. Elimelech, *Prediction of DLVO interaction energy and particle deposition rates for rough surfaces.* Abstracts of Papers of the American Chemical Society, 1997. **214**: p. 40-COLL.
60. Suresh, L. and J.Y. Walz, *Effect of Surface Roughness on the Interaction Energy between a Colloidal Sphere and a Flat Plate.* Journal of Colloid and Interface Science, 1996. **183**(1): p. 199-213.
61. Hoek, E.M.V., S. Bhattacharjee, and M. Elimelech, *Effect of membrane surface roughness on colloid-membrane DLVO interactions.* Langmuir, 2003. **19**(11): p. 4836-4847.
62. Israelacvili, J.N., *Intermolecular and Surface Forces*. 2007, London.
63. Weetman, P., S. Goldman, and C.G. Gray, *Use of the Poisson-Boltzmann Equation To Estimate The Electrostatic Free Energy Barrier for Dielectric*

Models of Biological Ion Channels. The Journal of Physical Chemistry B, 1997. **101**(31): p. 6073-6078.

64. van Oss, C.J., *Acid--base interfacial interactions in aqueous media.* Colloids and Surfaces A: Physicochemical and Engineering Aspects, 1993. **78**: p. 1-49.
65. de Gennes, P.G., *Polymers at an interface; a simplified view.* Advances in Colloid and Interface Science, 1987. **27**(3-4): p. 189-209.
66. Goren, S.L., *The hydrodynamic force resisting the approach of a sphere to a plane wall in slip flow.* Journal of Colloid and Interface Science, 1973. **44**(2): p. 356-360.
67. Happel, J., *Viscous flowin multiparticle systems: slow motion of fluids relative to beds of spherical particles.* AIChE J., 1958. **4**: p. 197-201.
68. Elimelech, M., Gregory, J., Jia, X., Williams, R.A., *Particle Deposition& Aggregation: Measurement, Modeling and Simulation.* 1995, Woburn, MA: Butterworth-Heinemann.
69. Van Oss, C.J., *Interfacial Forces in Aqueous Media.* 1994, New York: Dekker.
70. Mahmood, T., et al., *A micromechanics approach for attachment and detachment of asymmetric colloidal particles.* Colloids and Surfaces A: Physicochemical and Engineering Aspects, 2000. **177**(2-3): p. 99-110.
71. Adamczyk, Z. and P. Weronski, *Application of the DLVO theory for particle deposition problems.* Advances in Colloid and Interface Science, 1999. **83**(1-3): p. 137-226.
72. Chen, J.Y., et al., *Role of spatial distribution of porous medium surface charge heterogeneity in colloid transport.* Colloids and Surfaces A: Physicochemical and Engineering Aspects, 2001. **191**(1-2): p. 3-15.
73. Clark, R.E., J.C. Boyd, and J.F. Moran, *New Principles Governing Tissue Reactivity of Prosthetic Materials.* Journal of Surgical Research, 1974. **16**(5): p. 510-522.
74. Haddad, R.J., S.D. Cook, and K.A. Thomas, *Current Concepts Review - Biological Fixation of Porous-Coated Implants.* Journal of Bone and Joint Surgery-American Volume, 1987. **69A**(9): p. 1459-1466.
75. Thomas, K.A. and S.D. Cook, *An Evaluation of Variables Influencing Implant Fixation by Direct Bone Apposition.* Journal of Biomedical Materials Research, 1985. **19**(8): p. 875-901.
76. Krupp, H., *Particle adhesion theory and experiment.* Advances in Colloid and Interface Science, 1967. **1**(2): p. 111-239.
77. Adamcyzk, Z., *Particle Deposition from Flowing Suspensions.* Colloids and Surfaces, 1989. **39**(1): p. 1-37.
78. Elimelech, M. and C.R. Omelia, *Effect of Particle-Size on Collision Efficiency in the Deposition of Brownian Particles with Electrostatic Energy Barriers.* Langmuir, 1990. **6**(6): p. 1153-1163.
79. Czarnecki, J., *The effects of surface inhomogeneities on the interactions in colloidal systems and colloid stability.* Advances in Colloid and Interface Science, 1985. **24**: p. 283-319.

80. Czarnecki, J. and P. Warszynski, *The evaluation of tangential forces due to surface inhomogeneties in the particle deposition process.* Colloids and Surfaces, 1987. **22**(2): p. 187-205.
81. Herman, M.C. and K.D. Papadopoulos, *Effects of asperities on the van der Waals and electric double-layer interactions of two parallel flat plates.* Journal of Colloid and Interface Science, 1990. **136**(2): p. 385-392.
82. Herman, M.C. and K.D. Papadopoulos, *A method for modeling the interactions of parallel flat plate systems with surface features.* Journal of Colloid and Interface Science, 1991. **142**(2): p. 331-342.
83. Suresh, L. and J.Y. Walz, *Direct Measurement of the Effect of Surface Roughness on the Colloidal Forces between a Particle and Flat Plate.* Journal of Colloid and Interface Science, 1997. **196**(2): p. 177-190.
84. Kostoglou, M. and A.J. Karabelas, *The effect of discrete surface charge on potential energy of repulsion between colloidal surfaces.* Journal of Colloid and Interface Science, 1992. **151**(2): p. 534-545.
85. Richard Bowen, W. and T.A. Doneva, *Atomic Force Microscopy Studies of Membranes: Effect of Surface Roughness on Double-Layer Interactions and Particle Adhesion.* Journal of Colloid and Interface Science, 2000. **229**(2): p. 544-549.
86. Baker, J.H., *Factors Affecting the Bacterial-Colonization of Various Surfaces in a River.* Canadian Journal of Microbiology, 1984. **30**(4): p. 511-515.
87. Beeftink, H.H. and P. Staugaard, *Structure and Dynamics of Anaerobic Bacterial Aggregates in a Gas-Lift Reactor.* Applied and Environmental Microbiology, 1986. **52**(5): p. 1139-1146.
88. Rosenberg, M.D., *Cell Guidance by Alterations in Monomolecular Films.* Science, 1963. **139**(355): p. 411-&.
89. Curtis, A.S.G. and M. Varde, *Control of Cell Behavior - Topological Factors.* Journal of the National Cancer Institute, 1964. **33**(1): p. 15-&.
90. Wojciakstothard, B., et al., *Activation of Macrophage-Like Cells by Multiple Grooved Substrata - Topographical Control of Cell Behavior.* Cell Biology International, 1995. **19**(6): p. 485-490.
91. Komaromy, A., et al., *Micro-structures modulate bacterial cell viability and attachment.* Microelectronic Engineering, 2009. **86**(4-6): p. 1431-1434.
92. Oh, Y.J., et al., *Micropatterning of bacteria on two-dimensional lattice protein surface observed by atomic force microscopy.* Ultramicroscopy, 2008. **108**(10): p. 1124-1127.
93. Diaz, C., P. Schilardi, and M.F.L. de Mele, *Influence of surface sub-micropattern on the adhesion of pioneer bacteria on metals.* Artificial Organs, 2008. **32**(4): p. 292-298.
94. Ploux, L., et al., *Opposite Responses of Cells and Bacteria to Micro/Nanopatterned Surfaces Prepared by Pulsed Plasma Polymerization and UV-Irradiation.* Langmuir, 2009. **25**(14): p. 8161-8169.
95. Martin, J.Y., et al., *Effect of Titanium Surface-Roughness on Proliferation, Differentiation, and Protein-Synthesis of Human Osteoblast-Like Cells (Mg63).*

Journal of Biomedical Materials Research, 1995. **29**(3): p. 389-401.
96. Curtis, A.S.G. and C.D. Wilkinson, *Reactions of cells to topography.* Journal of Biomaterials Science-Polymer Edition, 1998. **9**(12): p. 1313-1329.
97. Whitehead, K.A., et al., *Use of the atomic force microscope to determine the effect of substratum surface topography on the ease of bacterial removal.* Colloids and Surfaces B-Biointerfaces, 2006. **51**(1): p. 44-53.
98. Diaz, C., et al., *Nano/Microscale order affects the early stages of Biofilm formation on metal surfaces.* Langmuir, 2007. **23**(22): p. 11206-11210.
99. Bhushan, B., *Biomimetics: lessons from nature - an overview.* Philosophical Transactions of the Royal Society a-Mathematical Physical and Engineering Sciences, 2009. **367**(1893): p. 1445-1486.
100. Barthlott, W. and C. Neinhuis, *Purity of the sacred lotus, or escape from contamination in biological surfaces.* Planta, 1997. **202**(1): p. 1-8.
101. Neinhuis, C. and W. Barthlott, *Characterization and distribution of water-repellent, self-cleaning plant surfaces.* Annals of Botany, 1997. **79**(6): p. 667-677.
102. Bechert, D.W., M. Bruse, and W. Hage, *Experiments with three-dimensional riblets as an idealized model of shark skin.* Experiments in Fluids, 2000. **28**(5): p. 403-412.
103. www.biomimicryinstitute.org.
104. Long, C.J., et al., *A model that predicts the attachment behavior of Ulva linza zoospores on surface topography.* Biofouling. **26**(4): p. 411-419.
105. Long, C.J., J.F. Schumacher, and A.B. Brennan, *Potential for tunable static and dynamic contact angle anisotropy on gradient microscale patterned topographies.* Langmuir, 2009. **25**(22): p. 12982-9.
106. www.sharklet.com.
107. Baum, C., et al., *Average nanorough skin surface of the pilot whale (Globicephala melas, Delphinidae): considerations on the self-cleaning abilities based on nanoroughness.* Marine Biology, 2002. **140**(3): p. 653-657.
108. Ball, P., *Engineering - Shark skin and other solutions.* Nature, 1999. **400**(6744): p. 507-+.
109. Wagner, T., C. Neinhuis, and W. Barthlott, *Wettability and contaminability of insect wings as a function of their surface sculptures.* Acta Zoologica, 1996. **77**(3): p. 213-225.
110. Genzer, J. and A. Marmur, *Biological and synthetic self-cleaning surfaces.* Mrs Bulletin, 2008. **33**(8): p. 742-746.
111. Bormashenko, E., et al., *Why do pigeon feathers repel water? Hydrophobicity of pennae, Cassie-Baxter wetting hypothesis and Cassie-Wenzel capillarity-induced wetting transition.* Journal of Colloid and Interface Science, 2007. **311**(1): p. 212-216.
112. Gu, Z.Z., et al., *Structural color and the lotus effect.* Angewandte Chemie-International Edition, 2003. **42**(8): p. 894-+.
113. Feng, L., et al., *Petal effect: A superhydrophobic state with high adhesive force.* Langmuir, 2008. **24**(8): p. 4114-4119.

114. Gao, X.F. and L. Jiang, *Water-repellent legs of water striders.* Nature, 2004. **432**(7013): p. 36-36.
115. del Campo, A. and E. Arzt, *Fabrication approaches for generating complex micro- and nanopatterns on polymeric surfaces.* Chemical Reviews, 2008. **108**(3): p. 911-945.
116. Flemming, R.G., et al., *Effects of synthetic micro- and nano-structured surfaces on cell behavior.* Biomaterials, 1999. **20**(6): p. 573-588.
117. Madou, M., *Fundamentals of microfabrication.* 1997, Boca Raton, New York: CRC Press.
118. Arden, W., *Optical Versus X-Ray-Lithography for Future Device Fabrication.* Microelectronic Engineering, Vol 13, 1991. **13**: p. 231-241.
119. Arden, W. and K.-H. M黷 ler, *Physical and technological limits in optical and x-ray lithography.* Microelectronic Engineering, 1987. **6**(1-4): p. 53-60.
120. Bertsch, A., H. Lorenz, and P. Renaud, *3D microfabrication by combining microstereolithography and thick resist UV lithography.* Sensors and Actuators A: Physical, 1999. **73**(1-2): p. 14-23.
121. Sun, H.B. and S. Kawata, *Two-photon photopolymerization and 3D lithographic microfabrication.* Nmr - 3d Analysis - Photopolymerization, 2004. **170**: p. 169-273.
122. Harris, T.W., *Chemical Milling.* 1976, Oxford: Clarendon Press.
123. An, Y.H. and R.J. Friedman, *Laboratory methods for studies of bacterial adhesion.* Journal of Microbiological Methods, 1997. **30**(2): p. 141-152.
124. Katsikogianni, M. and Y.F. Missirlis, *Concise review of mechanisms of bacterial adhesion to biomaterials and of techniques used in estimating bacteria-material interactions.* Eur Cell Mater, 2004. **8**: p. 37-57.
125. Liu, Y., *Adhesion kinetics of nitrifying bacteria on various thermoplastic supports.* Colloids and Surfaces B: Biointerfaces, 1995. **5**(5): p. 213-219.
126. Sadr Ghayeni, S.B., et al., *Adhesion of waste water bacteria to reverse osmosis membranes.* Journal of Membrane Science, 1998. **138**(1): p. 29-42.
127. Bos, R., H.C. van der Mei, and H.J. Busscher, *Physico-chemistry of initial microbial adhesive interactions - its mechanisms and methods for study.* Fems Microbiology Reviews, 1999. **23**(2): p. 179-230.
128. Leenaars, A.F.M., *A new approach to the removal of sub-micron particles from solid (silicon) substrates*
In: Particles on Surfaces, Detection, Adhesion and Removal, ed. K.L. Mittal. 1988, New York: Plenum Press. 361-372.
129. Leenaars, A.F.M. and S.B.G. Obrien, *Particle Removal from Silicon Substrates Using Surface-Tension Forces.* Philips Journal of Research, 1989. **44**(2-3): p. 183-209.
130. Visser, J., *Adhesion of colloidal particles*, in *Surface and Colloid Science*, E. Marijevic, Editor. 1976, John Wiley and Sons: New York. p. 3-84.
131. Rutter, P.R.V., B., *Attachment mechanisms in the surface growth of microorganisms*, in *Physiological Models in Microbiology*, M. Bazin, J.; Prosser, J.I., Editor. 1988, CRC Press: Boca Raton, FL. p. 87-107.

132. Krimmer, V., et al., *Detection of Staphylococcus aureus and Staphylococcus epidermidis in clinical samples by 16S rRNA-directed in situ hybridization.* Journal of Clinical Microbiology, 1999. **37**(8): p. 2667-2673.
133. Moter, A. and U.B. Gobel, *Fluorescence in situ hybridization (FISH) for direct visualization of microorganisms.* Journal of Microbiological Methods, 2000. **41**(2): p. 85-112.
134. Herbert, R.A., *Methods for Enumerating Microorganisms and Determining Biomass in Natural Environments.* Methods in Microbiology, 1990. **22**: p. 1-39.
135. Gabriel, M.M., et al., *In vitro evaluation of the efficacy of a silver-coated catheter.* Current Microbiology, 1996. **33**(1): p. 1-5.
136. Pringle, J.H. and M. Fletcher, *Influence of Substratum Wettability on Attachment of Fresh-Water Bacteria to Solid-Surfaces.* Applied and Environmental Microbiology, 1983. **45**(3): p. 811-817.
137. Mackowiak, P.A. and M. Marlingcason, *A Comparative-Analysis of Invitro Assays of Bacterial Adherence.* Journal of Microbiological Methods, 1984. **2**(3): p. 147-158.
138. Kefford, B. and K.C. Marshall, *Adhesion of Leptospira at a Solid-Liquid Interface - a Model.* Archives of Microbiology, 1984. **138**(1): p. 84-88.
139. Pascual, A., et al., *Modulation of Adherence of Coagulase-Negative Staphylococci to Teflon Catheters Invitro.* European Journal of Clinical Microbiology & Infectious Diseases, 1986. **5**(5): p. 518-522.
140. Timmerman, C.P., et al., *Characterization of a Proteinaceous Adhesin of Staphylococcus-Epidermidis Which Mediates Attachment to Polystyrene.* Infection and Immunity, 1991. **59**(11): p. 4187-4192.
141. Stellmach, J. and E. Severin, *A Fluorescent Redox Dye - Influence of Several Substrates and Electron Carriers on the Tetrazolium Salt Formazan Reaction of Ehrlich Ascites Tumor-Cells.* Histochemical Journal, 1987. **19**(1): p. 21-26.
142. Rodriguez, G.G., et al., *Use of a Fluorescent Redox Probe for Direct Visualization of Actively Respiring Bacteria.* Applied and Environmental Microbiology, 1992. **58**(6): p. 1801-1808.
143. McDowell, S.G., et al., *Application of a Fluorescent Redox Dye for Enumeration of Metabolically Active Bacteria on Albumin-Coated Titanium Surfaces.* Letters in Applied Microbiology, 1995. **21**(1): p. 1-4.
144. Rutter, P.R. and A. Abbott, *Study of Interaction between Oral Streptococci and Hard Surfaces.* Journal of General Microbiology, 1978. **105**(APR): p. 219-226.
145. Fletcher, M., *Methods for Studying Adhesion and Attachment to Surfaces.* Methods in Microbiology, 1990. **22**: p. 251-283.
146. Shea, C. and J.C. Williamson, *Rapid Analysis of Bacterial Adhesion in a Microplate Assay.* Biotechniques, 1990. **8**(6): p. 610-611.
147. Kubitschek, H.E., *Electronic Counting and Sizing of Bacteria.* Nature, 1958. **182**(4630): p. 234-235.
148. Chang, C.C. and K. Merritt, *Microbial Adherence on Poly(Methyl*

Methacrylate) (Pmma) Surfaces. Journal of Biomedical Materials Research, 1992. **26**(2): p. 197-207.

149. Robrish, S.A., C.W. Kemp, and W.H. Bowen, *Use of Extractable Adenosine-Triphosphate to Estimate Viable Cell Mass in Dental Plaque Samples Obtained from Monkeys.* Applied and Environmental Microbiology, 1978. **35**(4): p. 743-749.
150. Paul, J.H. and G.I. Loeb, *Improved Microfouling Assay Employing a DNA-Specific Fluorochrome and Polystyrene as Substratum.* Applied and Environmental Microbiology, 1983. **46**(2): p. 338-343.
151. Watson, S.W., et al., *Determination of Bacterial Number and Biomass in Marine-Environment.* Applied and Environmental Microbiology, 1977. **33**(4): p. 940-946.
152. Deupree, S.M. and M.H. Schoenfisch, *Quantitative method for determining the lateral strength of bacterial adhesion and application for characterizing adhesion kinetics.* Langmuir, 2008. **24**(9): p. 4700-4707.
153. Busscher, H.J., A.T. Poortinga, and R. Bos, *Lateral and perpendicular interaction forces involved in mobile and immobile adhesion of microorganism on model solid surfaces.* Current Microbiology, 1998. **37**(5): p. 319-323.
154. Beach, E.R., et al., *Pull-off force measurements between rough surfaces by atomic force microscopy.* Journal of Colloid and Interface Science, 2002. **247**(1): p. 84-99.
155. Butt, H.J., B. Cappella, and M. Kappl, *Force measurements with the atomic force microscope: Technique, interpretation and applications.* Surface Science Reports, 2005. **59**(1-6): p. 1-152.
156. Yamamoto, A., et al., *A new technique for direct measurement of the shear force necessary to detach a cell from a material.* Biomaterials, 1998. **19**(7-9): p. 871-879.
157. Shahin, V., et al., *Glucocorticoids remodel nuclear envelope structure and permeability.* Journal of Cell Science, 2005. **118**(13): p. 2881-2889.
158. Kusakabe, H., et al., *Osseointegration of a hydroxyapatite-coated multilayered mesh stem.* Biomaterials, 2004. **25**(15): p. 2957-2969.
159. Zreiqat, H. and C.R. Howlett, *Titanium substrata composition influences osteoblastic phenotype: In vitro study.* Journal of Biomedical Materials Research, 1999. **47**(3): p. 360-366.
160. Ferris, D.M., et al., *RGD-coated titanium implants stimulate increased bone formation in vivo.* Biomaterials, 1999. **20**(23-24): p. 2323-2331.
161. Morra, M. and C. Cassinelli, *Organic surface chemistry on titanium surfaces via thin film deposition.* Journal of Biomedical Materials Research, 1997. **37**(2): p. 198-206.
162. Horbett, T.A., et al., *Cell-Adhesion to a Series of Hydrophilic-Hydrophobic Copolymers Studied with a Spinning Disk Apparatus.* Journal of Biomedical Materials Research, 1988. **22**(5): p. 383-404.
163. Bausch, A.R., et al., *Local measurements of viscoelastic parameters of*

adherent cell surfaces by magnetic bead microrheometry. Biophysical Journal, 1998. **75**(4): p. 2038-2049.

164. de Kerchove, A.J. and M. Elimelech, *Impact of alginate conditioning film on deposition kinetics of motile and nonmotile Pseudomonas aeruginosa strains.* Applied and Environmental Microbiology, 2007. **73**(16): p. 5227-5234.
165. de Kerchove, A.J., P. Weronski, and M. Elimelech, *Adhesion of nonmotile Pseudomonas aeruginosa on "soft" polyelectrolyte layer in a radial stagnation point flow system: Measurements and model predictions.* Langmuir, 2007. **23**: p. 12301-12308.
166. Kuznar, Z.A. and M. Elimelech, *Adhesion Kinetics of Viable Cryptosporidium parvum Oocysts to Quartz Surfaces.* Environmental Science & Technology, 2004. **38**(24): p. 6839-6845.
167. Redman, J.A., S.L. Walker, and M. Elimelech, *Bacterial Adhesion and Transport in Porous Media:Role of the Secondary Energy Minimum.* Environmental Science & Technology, 2004. **38**(6): p. 1777-1785.
168. Walker, S.L., J.A. Redman, and M. Elimelech, *Role of Cell Surface Lipopolysaccharides in Escherichia coli K12 Adhesion and Transport.* Langmuir, 2004. **20**(18): p. 7736-7746.
169. de Kerchove, A.J. and M. Elimelech, *Calcium and Magnesium Cations Enhance the Adhesion of Motile and Nonmotile Pseudomonas aeruginosa on Alginate Films.* Langmuir, 2008. **24**(7): p. 3392-3399.
170. Kerchove, A.J.d. and M. Elimelech, *Bacterial Swimming Motility Enhances Cell Deposition and Surface Coverage.* Environmental Science & Technology, 2008. **42**(12): p. 4371-4377.
171. Sjollema, J., H.J. Busscher, and A.H. Weerkamp, *Experimental Approaches for Studying Adhesion of Microorganisms to Solid Substrata - Applications and Mass-Transport.* Journal of Microbiological Methods, 1989. **9**(2): p. 79-90.
172. Dickinson, R.B., et al., *Quantitative Comparison of Clumping Factor-Mediated and Coagulase-Mediated Staphylococcus-Aureus Adhesion to Surface-Bound Fibrinogen under Flow.* Infection and Immunity, 1995. **63**(8): p. 3143-3150.
173. Reutelingsperger, C.P.M., et al., *The Rotating-Disc as a Device to Study the Adhesive Properties of Endothelial-Cells under Differential Shear Stresses.* Journal of Materials Science-Materials in Medicine, 1994. **5**(6-7): p. 361-367.
174. http://rsbweb.nih.gov/ij/.
175. Ma, M.L. and R.M. Hill, *Superhydrophobic surfaces.* Current Opinion in Colloid & Interface Science, 2006. **11**(4): p. 193-202.
176. Patankar, N.A., *Mimicking the lotus effect: Influence of double roughness structures and slender pillars.* Langmuir, 2004. **20**(19): p. 8209-8213.
177. Marmur, A., *The lotus effect: Superhydrophobicity and metastability.* Langmuir, 2004. **20**(9): p. 3517-3519.
178. Waghorn, G.C., et al., *The Effect of Condensed Tannins on the Site of Digestion of Amino-Acids and Other Nutrients in Sheep Fed on*

Lotus-Corniculatus L. British Journal of Nutrition, 1987. **57**(1): p. 115-126.
179. Gao, L.C. and T.J. McCarthy, *The "lotus effect" explained: Two reasons why two length scales of topography are important.* Langmuir, 2006. **22**(7): p. 2966-2967.
180. Muler, F., et al., *Self-Cleaning Surfaces Using the Lotus Effect*, in *Handbook for Cleaning/Decontamination of Surfaces*. 2007, Elsevier Science B.V.: Amsterdam. p. 791-811.
181. Koch, K. and H.-J. Ensikat, *The hydrophobic coatings of plant surfaces: Epicuticular wax crystals and their morphologies, crystallinity and molecular self-assembly.* Micron, 2008. **39**(7): p. 759-772.
182. Guo, Z., W. Liu, and B.-L. Su, *Superhydrophobic surfaces: From natural to biomimetic to functional.* Journal of Colloid and Interface Science. **353**(2): p. 335-355.
183. Zhang, J.H., X.L. Sheng, and L. Jiang, *The Dewetting Properties of Lotus Leaves.* Langmuir, 2009. **25**(3): p. 1371-1376.
184. Cheng, Y.T. and D.E. Rodak, *Is the lotus leaf superhydrophobic?* Applied Physics Letters, 2005. **86**(14).
185. Verran, J., Boyd, R D, *The relationship between substratum surface roughness and microbiological and organic soiling: A review.* Biofouling, 2001. **17**: p. 59-71.
186. Amsler, C.D., D.C. Reed, and M. Neushul, *The Microclimate Inhabited by Macroalgal Propagules.* British Phycological Journal, 1992. **27**(3): p. 253-270.
187. Crisp, D.J., *Factors influencing the settlement of marine invertebrate larvae.* Chemoreception in Marine Organisms., ed. P.T. Grant, Mackie, A M. 1974, New York: Academic Press. 165-177.
188. Fletcher, R.L. and M.E. Callow, *The Settlement, Attachment and Establishment of Marine Algal Spores.* British Phycological Journal, 1992. **27**(3): p. 303-329.
189. Allion, A., J.P. Baron, and L. Boulange-Petermann, *Impact of surface energy and roughness on cell distribution and viability.* Biofouling, 2006. **22**(5): p. 269-278.
190. Whitehead, K.A., J. Colligon, and J. Verran, *Retention of microbial cells in substratum surface features of micrometer and sub-micrometer dimensions.* Colloids and Surfaces B-Biointerfaces, 2005. **41**(2-3): p. 129-138.
191. Callow, M.E., et al., *Microtopographic cues for settlement of zoospores of the green fouling alga Enteromorpha.* Biofouling, 2002. **18**(3): p. 237-245.

Appendix. Nomenclature

Nomenclature

A_H	Hamaker constant(0.8×10^{-20}J)
d	size of the pillar (square side)
dA	differential area of a surface element
D	separation distance of the sphere from the patterned surface
H	height of the micro-pillars
k	Boltzmann constant
s	spacing between micro-pillars
T	absolute temperature
U(D)	total DLVO interaction energy
$U_{plane}(H)$	interaction energy per unit area between two infinite plannar surfaces
$U_{EDL}(H)$	electrostatic double-layer interaction energy per unit area
UVDW(H)	van der Waals interaction energy per unit area
kT	pseudo-unit of energy ($4.11\text{x}10^{-21}$ J)
Greek symbols	
ε	dielectric constant of water (78.5)
ε_0	dielectric permittivity of vacuum ($8.854\text{x}10^{-12}$)
ζ	zeta-potential of a flat plate
κ	inverse Debye length
$\psi_{01/02}$	surface potentials of flat plates
γ	interfacial free energy
coth(x)	hyperbolic cotangent ($\coth(x)=\frac{\sinh(x)}{\cosh(x)}=\frac{e^x-e^{-x}}{e^x+e^{-x}}$)
cosech(x)	hyperbolic cosecant ($\mathrm{cosech}(x)=(\sinh(x))^{-1}=\frac{2}{e^x-e^{-x}}$)